Long term stable integration of a maximally sliced Schwarzschild black hole using a smooth lattice method

Leo Brewin

Department of Mathematics & Statistics
Monash University
Clayton, Vic. 3800
Australia
22-Jun-2001

arXiv:gr-qc/0107030v1 10 Jul 2001

Abstract

We will present results of a numerical integration of a maximally sliced Schwarzschild black hole using a smooth lattice method. The results show no signs of any instability forming during the evolutions to $t = 1000m$. The principle features of our method are i) the use of a lattice to record the geometry, ii) the use of local Riemann normal coordinates to apply the 1+1 ADM equations to the lattice and iii) the use of the Bianchi identities to assist in the computation of the curvatures. No other special techniques are used. The evolution is unconstrained and the ADM equations are used in their standard form.

PACS numbers: 04.25.Dm, 04.60.Nc, 02.70.-c

1. Introduction

Recent studies [1–7] have shown that the stability of numerical integrations of the Einstein field equations can depend on the formulation of the evolution equations. Subtle changes in the structure of the evolution equations have been shown to have a dramatic effect on the long term stability of the integrations. These are relatively new investigations and thus at present there is no precise mathematical explanation as to what is the root cause of the instabilities or how best they can be avoided or minimised. What we have at present is a growing set of examples which suggests that the standard ADM evolution equations may not be the most suitable equations for numerical relativity. Consequently many people are looking at alternative formulations such as the hyperbolic formulations of Einstein's equations [8–10] and the conformal ADM equations of Shibita and Nakamura [6] and Baumgarte and Shapiro [3].

One alternative is the smooth lattice approach which we presented in two earlier papers [11,12]. This is a method which uses a lattice similar to that used in the Regge calculus but differing significantly in the way the field equations are imposed on the lattice. In the smooth lattice method we employ a series of local Riemann normal coordinates in which the connection vanishes at the origin of each such frame. Collectively these frames enable us to obtain point estimates of the curvatures in terms of the lattice data (in particular the leg lengths). The upshot is that the 3+1 ADM equations can be applied directly to the lattice.

This is clearly a radically different approach to that normally used in numerical relativity. It is thus interesting to explore its stability properties against those for traditional techniques.

In our first paper [11] we showed how the smooth lattice method could be used to obtain the initial data for a Schwarzschild spacetime. In the second paper [12] we showed how the 3+1 ADM equations could be applied to a lattice using the Kasner spacetime as a test case. In both papers the results were very encouraging. In this paper we return to the Schwarzschild spacetime, this time to study the stability of its evolution in a maximal guage.

Studies of a maximally sliced Schwarzschild spacetimes in spherical symmetry were quite popular some years ago (see for example [13,14]). These studies showed that the evolutions were invariably unstable. The source of the instability was attributed to the stretching of the grid as grid points nearer the black hole were drawn into the black hole quicker than those further out. With the consequent loss of resolution the estimates for the derivatives were seriously in error and the non-linear feedback in the equations quickly drove the solution into exponential overflow.

We will repeat these calculations using our smooth lattice method so that we can address the simple questions : When will the loss of resolution become apparent, what impact will it have on the subsequent evolution and will it trigger an unstable evolution?

We should point out that this paper is not an attempt to revive the use of maximal slicing as a preferred slicing condition. We are, instead, using it solely as a test of the smooth lattice method.

We will try to stay as close as possible to the earlier work of Bernstein, Hobill and Smarr [14]. Thus we shall not be using any of the modern techniques, such as apparent horizon boundary conditions [15], conformal differentiation [16] and using the Hamiltonian constraint to stabilise the maximal slicing equation [13]. We will, however, employ some techniques of our own, in particular we will use a lattice to record the metric, we will cover the lattice with a series of local frames and we will use the Bianchi identities in computing the curvatures.

As this method may be unfamiliar to many readers we have included more details of the derivations than might normally be included. However, to spare the reader we have relegated the bulk of the derivations to a (large) appendix. The sections that precede the appendix contain all of the important results with few derivations. We begin with a brief review of the smooth lattice method, followed by a description of the particular lattice used for the Schwarzschild spacetime. We then present the details of the 1+1 ADM equations, the results of the integrations and finally we review what we have found.

2. Riemann Normal Coordinates and Smooth Lattices

The concept of a smooth lattice was first introduced by Brewin [11,12] as a method by which a discrete lattice could be coupled to a family of Riemann normal frames in such a way as to provide smooth estimates for the metric and curvature on the lattice.

The principle features of the smooth lattice method are

- ◇ The lattice is a finite collection of vertices and legs connected in any suitable fashion (e.g. a simplicial lattice).
- ◇ The data recorded on the lattice is purely geometrical, such as the leg lengths and angles between pairs of legs.
- ◇ To each vertex their is assigned a small neighbourhood in which local Riemann normal coordinates are employed. Each such neighbourhood is called a computational cell. For a simplicial lattice the computational cell can be chosen as the set of simplicies attached to the central vertex.
- ◇ The legs of a computational cell are taken as geodesic segments of a locally smooth metric.
- ◇ The leg lengths are small compared to the curvature length scales, that is, $RL^2 << 1$ where R and L typical values for the curvature and leg lengths respectively.

There are a number of equivalent definitions of Riemann normal coordinates [17,18,19,20]. One definition has them to be the coordinates which, for a given point P, the geodesics through P are all of the form $x^\mu(s) = sa^\mu$ where s is an affine parameter and the a^μ are constants (i.e. they are "straight" lines). The coordinates of a point Q near P are then taken as $x^\mu(s)$ for the geodesic that joins P to Q. Clearly this restricts the region in which these coordinates can be used to that for which there is a unique geodesic which joins P to Q. In larger regions it is possible that pairs of geodesics may cross and thus the coordinates at the intersection would not be unique. This problem is avoided in a smooth lattice by requiring the leg lengths to be small when compared to the curvature length scales, i.e. $RL^2 << 1$.

An equivalent definition of Riemann normal coordinates is that the connection and its symmetric first derivative vanish at P,

$$0 = \Gamma^\mu{}_{\alpha\beta} \tag{2.1}$$

$$0 = \Gamma^\mu{}_{\alpha\beta,\lambda} + \Gamma^\mu{}_{\beta\lambda,\alpha} + \Gamma^\mu{}_{\lambda\alpha,\beta} \tag{2.2}$$

In a Riemann normal frame it is relatively easy to show that the metric, when expanded about the point P, takes the form

$$g_{\mu\nu}(x) = g_{\mu\nu} - \frac{1}{3}R_{\mu\alpha\nu\beta}x^\alpha x^\beta + \mathcal{O}(x^3) \tag{2.3}$$

where $g_{\mu\nu}$ are constants that can always be chosen to be $\mathrm{diag}(1,1,1)$. This prescription does not uniquely determine the coordinates as rotations around P are still allowed. This guage freedom can be used to orient the axes to preferred edges of the lattice.

From this form of the metric it is relatively easy to compute various geometrical quantities such as the geodesic length L_{ij} between two vertices i and j

$$L_{ij}^2 = g_{\mu\nu}\Delta x_{ij}^\mu \Delta x_{ij}^\nu - \frac{1}{3}R_{\mu\alpha\nu\beta}x_i^\mu x_i^\nu x_j^\alpha x_j^\beta + \mathcal{O}(\epsilon^5) \tag{2.4}$$

and the angle θ_i subtended at the vertex i in the geodesic triangle (ijk)

$$2L_{ij}L_{ik}\cos\theta_i = L_{ij}^2 + L_{ik}^2 - L_{jk}^2 - \frac{1}{3}R_{\mu\alpha\nu\beta}\Delta x_{ij}^\mu \Delta x_{ij}^\nu \Delta x_{ik}^\alpha \Delta x_{ik}^\beta + \mathcal{O}(\epsilon^5) \tag{2.5}$$

In these equations x_i^μ are the coordinates of vertex i, $\Delta x_{ij}^\mu = x_i^\mu - x_j^\mu$ and ϵ is a typical (small) length scale. See [11] for a derivation of these equations.

The principle advantages of using a smooth lattice method over other lattice methods are

- ◇ The metric is smooth and differentiable.
- ◇ Point estimates of the curvatures are easy to compute.
- ◇ The equivalence principle is explicitly used in each computational cell.
- ◇ The vanishing of the connection at a vertex greatly simplifies many equations (i.e. covariant differentiation reduces to partial differentiation).

3. The lattice

The smooth lattice method could equally be applied to the 4-dimensional spacetime or, in a 3+1 ADM context, to each spacelike Cauchy surface. We will adopt the second approach simply because it reduces the complexity of the bookkeeping (a 3-d computational cell has far less complexity than its 4-d counterpart). The 3+1 ADM equations will be used to evolve the 3-d smooth lattice.

For a Schwarzschild spacetime it is reasonable to choose the Cauchy surface to be a lattice built upon concentric 2-spheres. Each two sphere could be subdivided into a set of cells (e.g. triangles) using the same pattern on every 2-sphere. The successive 2-spheres can be joined by short radial legs connecting pairs of similar vertices. This construction is not unique as it does allow for a creeping rotation to occur between successive 2-spheres. This can be eliminated by demanding that the radial legs be perpendicular to the 2-spheres.

As part of the smooth lattice approach we require each leg in the lattice to be a geodesic segment of the 3-metric. Thus, as the radial legs are required to be normal to each 2-sphere, we see that each sequence of connected radial legs also forms a global geodesic of the 3-metric.

What flexibility do we have in choosing the leg lengths? Since the space must by spherically symmetric we can only adjust the overall scale of each two sphere and the distance between successive 2-spheres. These two pieces of information can be recorded by specifying the leg lengths between a pair of 2-spheres, L_{zz}, and the typical length within a 2-sphere, L_{xx}. By this means we can reduce the complexity of a full 3-dimensional lattice to a simple 2-dimensional ladder as indicated in figure 2.

3.1. The computational cell

Each Riemann normal frame was chosen to cover the region between three consecutive 2-spheres. Thus each Riemann normal frame will include the three rungs L^{+}_{xx}, L°_{xx}, L^{-}_{xx} and the two struts L^{+}_{zz} and L^{-}_{zz}. We also chose to align each Riemann normal frame so that i) the ladder was confined to the xz-plane, ii) the z-axis coincided with the familiar radial axis and iii) the z-axis threaded the mid-points of each rung (see figures (1,2,3)). It follows that the coordinates of the vertices must be of the following form

Table 1. Coordinates for the vertices in Figure 3

Vertex	(x,y,z)	**Vertex**	(x,y,z)	**Vertex**	(x,y,z)
1^{-}	$(\ u^{-},\ 0,\ v^{-})$	1	$(\ u^{\circ},\ 0,\ 0)$	1^{+}	$(\ u^{+},\ 0,\ v^{+})$
2^{-}	$(-u^{-},\ 0,\ v^{-})$	2	$(-u^{\circ},\ 0,\ 0)$	2^{+}	$(-u^{+},\ 0,\ v^{+})$

with $v^{-} < 0$ and $v^{+} > 0$. Note that the origin of the Riemann normal frame has been located (by a translation in the radial direction) so that the z coordinate of vertices 1 and 2 are zero.

We also require that successive pairs of struts form a global radial geodesic, that is, there can be no kink at the vertex where the radial struts meet. Thus we demand that

$$\pi = \theta^{+} + \theta^{-} \tag{3.1.1}$$

which we call the geodesic constraint. From these five leg lengths and one geodesic constraint we need to compute the curvatures and all of the coordinates (see section 8.1 for details).

3.2. The Riemann curvatures

For a spherically symmetric space there are just two algebraically independent curvature terms, R_{xyxy} and $R_{xzxz} = R_{yzyz}$ (the equality arises from the rotational symmetry around the z-axis). In Appendix 8.1 we show that the system of equations for the leg lengths and the geodesic constraint can be reduced to a single equation for R_{xzxz}

$$0 = \frac{2}{L^{+}_{zz} + L^{-}_{zz}} \left(\frac{L^{+}_{xx} - L^{\circ}_{xx}}{L^{+}_{zz}} + \frac{L^{-}_{xx} - L^{\circ}_{xx}}{L^{-}_{zz}} \right) + R_{xzxz} L^{\circ}_{xx} \tag{3.2.1}$$

which in turn is seen to be a finite difference approximation (on a non-uniform lattice) to the geodesic deviation equation for nearby radial geodesics, namely

$$0 = \frac{d^2 L_{xx}}{dz^2} + R_{xzxz} L_{xx} \tag{3.2.2}$$

The remaining smooth lattice equations serve only to determine the coordinates u°, u^+, etc. Clearly we need one more equation in order to compute the second curvature R_{xyxy}. This could be obtained by introducing extra structure into the lattice, such as the diagonal braces joining pairs of vertices on a 2-sphere. In fact this structure already exists – when we first spoke of the lattice we imagined each 2-sphere to be fully triangulated. Only later latter did we choose one of the legs on which to build our ladder. We could simply choose the collection of triangles attached to a particular vertex as a base on which to build a more sophisticated lattice with one ladder built over each leg of each triangle. This lattice would contain two classes of ladders – those sharing the common radial geodesic (that generated by the central vertex) and a chain of ladders forming a cylinder around the common radial geodesic. This lattice would therefore contain two classes of rungs – one for each class of ladder. In principle this lattice should allow us to compute both curvatures, R_{xzxz} and R_{xyxy}. However, there is a further complexity in that we do not know, a priori, the relationship between the leg lengths of the two classes of rungs. One might be tempted to set the lengths of each class of rung in the asymptotically flat region (i.e. far from the throat) and to then impose the same ratios (between the two classes) for all of the rungs back down to the throat. This would be correct if the rungs of the ladders where geodesic segments of each 2-sphere. However, the rungs are geodesic segments of the full 3-dimensional metric and thus their ratios will change with distance from the black hole's throat. Rather than pursue a solution to this problem we chose instead to retain our simple (one ladder) lattice and to employ the Bianchi identities to compute the second curvature R_{xyxy}. For our spherically symmetric space we can show (see Appendix 8.7) that there is only one non-trivial Bianchi identity

$$0 = \frac{\left(L_{xx}^2 R_{xyxy}\right)^+ - \left(L_{xx}^2 R_{xyxy}\right)^\circ}{L_{zz}^+} - \frac{1}{2}\left(R_{xzxz}^+ + R_{xzxz}^\circ\right) \frac{\left(L_{xx}^2\right)^+ - \left(L_{xx}^2\right)^\circ}{L_{zz}^+} \tag{3.2.3}$$

which is is a simple forward finite difference approximation to the continuum equation

$$0 = \frac{d\left(L_{xx}^2 R_{xyxy}\right)}{dz} - R_{xzxz} \frac{dL_{xx}^2}{dz} \tag{3.2.4}$$

in which z is the proper distance measured along the radial axis from the throat.

We solve the coupled equations (3.2.1,3.2.3) for the curvatures given all the leg lengths and a suitable initial value for R_{xyxy} on the inner boundary of the lattice (see section 5 for details).

4. The 1+1 ADM equations

4.1. The evolution equations

In an earlier paper [12] we showed how the 3+1 ADM evolution equations may be applied to any lattice. For the present problem with zero shift and drift the evolution equations may be written (see Appendix 8.2) as

$$\frac{dL_{ij}^2}{dt} = -2NK_{\mu\nu}\Delta x_{ij}^{\mu}\Delta x_{ij}^{\nu} \tag{4.1.1}$$

$$\frac{d}{dt}\left(K_{\mu\nu}\Delta x_{ij}^{\mu}\Delta x_{ij}^{\nu}\right) = \left(-N_{|\mu\nu} + N\left(R_{\mu\nu} + KK_{\mu\nu} - 2K_{\mu\alpha}K_{\nu}^{\alpha}\right)\right)\Delta x_{ij}^{\mu}\Delta x_{ij}^{\nu} \tag{4.1.2}$$

which when applied to our lattice (see Appendix 8.2) leads to

$$\frac{dL_{xx}}{dt} = -NK_{xx}L_{xx} \tag{4.1.3}$$

$$\frac{dL_{zz}}{dt} = -NK_{zz}L_{zz} \tag{4.1.4}$$

$$\frac{dK_{xx}}{dt} = -N_{,xx} + N\left(R_{xx} + KK_{xx}\right) \tag{4.1.5}$$

$$\frac{dK_{zz}}{dt} = -N_{,zz} + N\left(R_{zz} + KK_{zz}\right) \tag{4.1.6}$$

where $K = 2K_{xx} + K_{zz}$, $R_{xx} := R^{\mu}{}_{x\mu x} = R_{xyxy} + R_{xzxz}$ and $R_{zz} := R^{\mu}{}_{z\mu z} = 2R_{xzxz}$. The partial derivatives of the lapse function $N_{,xx}$ and $N_{,zz}$ can be evaluated using the techniques in Appendix 8.5, leading to

$$N_{,xx} = \frac{1}{L_{xx}}\frac{dL_{xx}}{dz}\frac{dN}{dz} \tag{4.1.7}$$

$$N_{,zz} = \frac{d^2N}{dz^2} \tag{4.1.8}$$

4.2. The constraint equations

For the Schwarzschild spacetime there are only two non-trivial constraint equations, the Hamiltonian constraint

$$0 = R + K^2 - K^{\mu\nu}K_{\mu\nu} \tag{4.2.1}$$

and the momentum constraint

$$0 = K_{|\mu} - K_{\mu}{}^{\nu}{}_{|\nu} \tag{4.2.2}$$

where $K = K^{\mu}{}_{\mu}$. These equations are readily adapted to the smooth lattice (see Appendix 8.6) leading to

$$0 = R_{xyxy} + 2R_{xzxz} + K_{xx}^2 + 2K_{xx}K_{zz} \tag{4.2.3}$$

$$0 = \frac{d\left(L_{xx}K_{xx}\right)}{dz} - K_{zz}\frac{dL_{xx}}{dz} \tag{4.2.4}$$

5. Numerical methods

5.1. The initial data

The initial data for the lattice consists of the leg lengths L_{xx}, L_{zz} and the extrinsic curvatures K_{xx}, K_{zz}. These can be freely chosen subject to the two constraints (4.2.3) and (4.2.4). For a time symmetric slice we must have $0 = K_{xx} = K_{zz}$ and consequently the momentum constraint (4.2.4) is identically satisfied. This leaves the Hamiltonian constraint, which now takes the simple form,

$$0 = R_{xyxy} + 2R_{xzxz} \tag{5.1.1}$$

as the one equation to constrain L_{xx} and L_{zz}. Following Bernstein, Hobill and Smarr [14] we chose to set L_{zz} while computing the L_{xx} as a solution of the Hamiltonian constraint.

The radial leg lengths L_{zz} where set as follows. A stretched grid of isotropic radial coordinates were defined by

$$r_j = \frac{m}{2}e^{(j\Delta)} \tag{5.1.2}$$

with $j = 0$ on the inner boundary (the throat) and $j = N$ on the outer boundary. The parameters Δ and N were chosen by Bernstein, Hobill and Smarr so that the outer boundary was at $r \approx 200m$. They chose $\Delta = 6/N$ and $N = 200$ while for our production runs we chose $N = 800$. The L_{zz} were then chosen as

$$L_{zz} = \int_{r_j}^{r_{j+1}} \left(1 + \frac{m}{2r}\right)^2 dr \tag{5.1.3}$$

for $j = 0$ to $j = N - 1$.

The L_{xx} were set by re-arranging the coupled system (3.2.1,3.2.3) and (5.1.1) in the form of a radial integration. Starting from the throat and working outwards,

$$L_{xx}^{+} = L_{xx}^{\circ} + \frac{L_{zz}^{+}}{L_{zz}^{-}}\left(L_{xx}^{\circ} - L_{xx}^{-}\right) + \frac{1}{4}L_{zz}^{+}\left(L_{zz}^{+} + L_{zz}^{-}\right)\left(L_{xx}R_{xyxy}\right)^{\circ} \tag{5.1.4}$$

$$R_{xyxy}^{+} = R_{xyxy}^{\circ}\left(\frac{5\left(L_{xx}^2\right)^{\circ} - \left(L_{xx}^2\right)^{+}}{5\left(L_{xx}^2\right)^{+} - \left(L_{xx}^2\right)^{\circ}}\right) \tag{5.1.5}$$

$$R_{xzxz}^{+} = -\frac{1}{2}R_{xyxy}^{+} \tag{5.1.6}$$

At the throat we imposed reflection symmetry by setting $L^{+}_{xx} = L^{-}_{xx}$, $L^{+}_{zz} = L^{-}_{zz}$. We also chose $L^{\circ}_{xx} = m/10$ (the equations are linear in L°_{xx} and thus this choice is not crucial) and $R^{\circ}_{xyxy} = 1/(4m^2) = -2R^{\circ}_{xzxz}$ (which we obtained from the analytic solution). Finally, we set $m = 1$. With this information we applied the above equations to generate all of the lattice data from the throat out to the outer boundary.

Is it reasonable to be using the analytic solution to assist us in setting the initial data? The only information borrowed from the analytic solution are the L_{zz} in each cell and R_{xyxy} at the throat. Where we chose to locate the successive Riemann cells is up to us, that is, we are free to choose the L_{zz} as we see fit. This is identical to the freedom to choose the lapse function when evolving the initial data. Thus this use of the analytic solution is not crucial and is made only to allow us to make direct comparisons with Bernstein, Hobill and Smarr. But what of the choice of curvature R_{xyxy}? Notice that the analytic solution depends on just one parameter, the mass m. Our lattice initial data also depends on just one parameter, the value of R_{xyxy} at the throat. Thus whatever choice we make for R_{xyxy} we are in effect choosing the ADM mass of our numerical spacetime. We could make some other choice for R_{xyxy} and then later determine the ADM mass for our numerical spacetime. To take this approach would be tedious and thus we chose to take the easier option where we set the ADM mass at the outset. Note that we make no further use of the analytic solution throughout the subsequent evolution.

5.2. The boundary conditions

The standard boundary conditions for Schwarzschild initial data are that the inner boundary is reflection symmetric and that in the distant regions the data is asymptotically flat. The reflection symmetry can be imposed by extending the lattice so as to have a computational cell that straddles the throat and then to demand that the two halves of this cell be mirror copies of each other. With this extra computational cell we can apply any of the lattice equations at the throat.

For a reflection symmetric throat we demand $L^{+}_{xx} = L^{-}_{xx}$ and $L^{+}_{zz} = L^{-}_{zz}$ at the throat. This condition was imposed throughout the evolution by setting L^{-}_{xx} and L^{-}_{zz} equal to their updated counterparts L^{+}_{xx} and L^{+}_{zz} at each stage of the integration (i.e. within each of the four steps of the 4th order Runge-Kutta).

At the outer boundary we extended the lattice by half a cell so that we could apply the evolution equations to the data associated with that cell. The data for the extra half cell were obtained by cubic extrapolation from the interior. The only data that needed to be extrapolated was K_{xx}, N, N_{zz} and R_{xzxz} for the grid centred scheme (see section (5.4)) and R_{xzxz} for the standard scheme. In both schemes we set $0 = dL^{+}_{xx}/dt$.

5.3. The lapse function

A maximally sliced spacetime is defined to be a spacetime for which $K = 0$ everywhere. This is normally imposed by setting $K = 0$ on the initial Cauchy surface and then setting $dK/dt = 0$ throughout the evolution. This condition leads, through the standard ADM evolution equations, to the following elliptic equation for the lapse function

$$0 = \nabla^2 N - RN \tag{5.3.1}$$

Using the results of section 8.5 we can write this as

$$0 = \frac{d^2N}{dz^2} + \frac{2}{L_{xx}}\frac{dL_{xx}}{dz}\frac{dN}{dz} - RN \tag{5.3.2}$$

which in turn can be applied to the lattice by replacing each of the derivatives by finite difference approximations on a non-uniform lattice (see Appendix 8.8)

The common wisdom is that to obtain a stable evolution, the Hamiltonian constraint should be used to eliminate the curvatures terms in the above equation. However, we found (see section 6) that the evolution was stable without this modification.

The boundary conditions of reflection symmetry at the throat, $dN/dz = 0$, and asymptotic flatness $\lim_{r\to\infty} N = 1$ were prescribed on our (finite) lattice as

$$\text{inner boundary :} \qquad 0 = N^{+} - N^{-} \tag{5.3.3}$$

$$\text{outer boundary :} \qquad 1 = N^{\circ} \tag{5.3.4}$$

The coupled system (5.3.2–5.3.4) were solved by three iterations of a shooting method. In each shot we made a guess $\widetilde{N}^{-}$ for N^{-} on the inner boundary and then used a Thomas algorithm to solve a modified system of equations consisting of $\widetilde{N}^{-} = N^{-}$ at the inner boundary, the main equation (5.3.2) everywhere on the lattice (except the outer boundary) and the outer boundary equation $1 = N^{\circ}$. The two initial guesses for N^{-} were taken as $\widetilde{N}^{-} = 0$ and $\widetilde{N}^{-} = 1$. After each shot, an estimate for dN/dz at the inner boundary was formed,

$$\frac{dN}{dz} = \frac{N^{+} - N^{-}}{2L_{zz}} \tag{5.3.5}$$

Since the equation (5.3.2) is linear in N it is possible to form a linear combination of the two solutions (one from each shot) so as to satisfy both the inner and outer boundary conditions. This leads to the third and final guess

$$\widetilde{N}_3^{-} = \left(\frac{dN}{dz}\right)_1 \left(\left(\frac{dN}{dz}\right)_1 - \left(\frac{dN}{dz}\right)_2\right)^{-1} \tag{5.3.6}$$

with the subscripts denoting the shot number. This guess was used for the final shot for the lapse on the lattice.

5.4. Time stepping

In each Riemann normal frame we can use the evolution equations to compute the time derivatives of the lattice data. However some of the lattice data are shared between neighbouring frames, L_{zz} for example, and thus we will obtain multiple estimates for their time derivatives. How then should we compute a single estimate for the time derivatives of the lattice data? Though there are many schemes which could be imposed, we chose two related schemes.

In the first scheme, which we will refer to as the standard scheme, we formed simple averages over all of the time derivatives for each component of the lattice data. For example, as each leg joins two vertices there will be two estimates available for its time derivative, one from each vertex. For some legs, such as L_{xx}, the two vertices are in equivalent frames (i.e. the two frames are at the same distance from the throat) and thus yield identical values for the time derivatives. Thus, for these legs it was sufficient to compute just the one time derivative. However, for legs such as L_{zz}, the two Riemann frames are distinct and both time derivatives must be computed. In the standard scheme no averaging was performed for the time derivatives of the $K_{\mu\nu}$.

In the second scheme we treat L_{zz} and K_{zz} as if they are defined at the centre of their associated legs. All other data, $L_{xx}, K_{xx}, R_{xyxy}, R_{xzxz}, N, N_{xx}, N_{zz}$ are taken to be defined on the vertices. When the time derivatives are evaluated, interpolations of the data are required to assemble all terms at the appropriate point. We take the average of the vertex data when interpolating from a pair of vertices to the centre of the leg. However, the interpolation of the data from the centres of the legs to the vertices is slightly more involved. For a function f defined at the centre of the radial legs the interpolation to the common vertex of two successive radial legs is given by

$$\widetilde{f} = \frac{1}{L^+_{zz} + L^-_{zz}} \left(L^+_{zz} f^- + L^-_{zz} f^+ \right) \tag{5.4.1}$$

This formula was only applied to the K_{zz} terms when computing the time derivatives for L_{xx} and K_{xx}. The final step was to take averages as per the standard scheme. This method will be referred to as the grid centred scheme.

One could ask why the L_{xx} and K_{xx} where not given a similar centred treatment. The answer is that, because of the rotational symmetry of the lattice, the interpolation would produce values identical to that obtained by assuming the L_{xx} were based on the vertices. So for simplicity we choose to take L_{xx} and K_{xx} as based on the vertices in the grid centred scheme.

For all of our production runs we chose a 4-th order Runge-Kutta scheme with a fixed time step of $\delta t = 0.01$. The evolution equations (4.1.3–4.1.6) were treated as a fully coupled system of equations.

In each of the four steps of a single Runge-Kutta cycle we would first compute all of the R_{xzxz} using (3.2.1). From (3.2.3) we would then compute the R_{xyxy}, from the throat to the outer boundary, using the Hamiltonian constraint (4.2.3) as a boundary condition for R_{xyxy} at the throat. Then followed the computation of the lapse function, the time derivatives and their averages before the partial updates were made. This would be repeated for the remaining steps in the Runge-Kutta cycle.

6. Results

The results of our integrations, using the grid centred scheme on a grid with 800 radial legs, are presented in figures (5–13). Notice that all of the curves are smooth and show no signs of any instabilities to $t = 1000m$. We have also marked the location of the apparent horizon on each curve with a diamond (the procedure for locating the apparent horizon is described later in section 6.5). This clearly shows that the horizon propagates smoothly and with almost constant speed across the grid. It is also clear that majority of the dynamics occurs within a very narrow region straddling the horizon.

The standard scheme produced curves that were qualitatively similar to those from the grid centred scheme. In particular they showed no signs of any numerical instabilities out to $t = 1000m$. They did, however, show non-trivial quantitative differences in the later stages of the evolution – at $t = 1000m$ the standard scheme's grid had stretched out to $739m$ as opposed to $826m$ for the grid centred scheme. The grid centred scheme also showed better constancy in the area of the apparent horizon (see section (6.5)), with only a 4% change in area from $t = 0$ to $t = 100m$ as opposed to a 13% change for the standard scheme. In the later stages of the evolution we can expect that the accuracy of the solution will be degraded due to the loss of resolution near the apparent horizon. This problem will occur with all numerical methods that do not provide for special treatment over the highly dynamical regions (e.g. an adaptive grid refinement scheme such as that due to Berger and Oliger [21]).

There are a number of simple checks that have been used by many others [13,14,16] to check the quality of the numerical solution. These include monitoring the constraints, the growth of the apparent horizon, the convergence of the maximal slices to $r = 3m/2$ and the so called *collapse of the lapse*. We will discuss each of these checks in turn.

6.1. Constraints

Ideally the constraints should remain bounded throughout the evolution. In practice though the constraints do drift away from their initial values. The plots in figures (11,12) do show an initial growth in the constraints but after $t \approx 100m$ the constraints remain bounded.

6.2. The $r = 3m/2$ limit

It has been shown by Estabrook etal [22] that the maximal slices of the Schwarzschild spacetime converge to the limit surface $r = 3m/2$ where in this case r is the standard Schwarzschild radial coordinate. We can use this as a check on our solution. Those parts of the grid for which the lapse has collapsed will be frozen on $r = 3m/2$. Thus the lattice data should be constant across those sections. This can be seen in the early stages of the evolution where inside the apparent horizon all of the data are (approximately) constant. For the curvature terms we can estimate what these constants should be. Notice that the geometry inside the apparent horizon is that of a cylinder, i.e. $S^2 \times R$. The scalar 3-curvature will be just that of the 2-curvature of the 2-dimensional cross sections (i.e of a 2-sphere of radius $r = 3m/2$). Thus we must have $R = 2/r^2$. We also know that $R = 2(R_{xyxy} + 2R_{xzxz})$ and as L^2_{xx} is constant along the cylinder we find from (3.2.2) that $R_{xzxz} = 0$. Thus we deduce that $R_{xyxy} = 4/(9m^2) = 0.\dot{4}/m^2$ which agrees well with our numerical value of $0.44445/m^2$ during the early evolution, from $t = 0$ to $t = 100m$. However, we loose agreement in the long term evolution, $t = 100m$ to $t = 1000m$. This is caused by a loss of resolution near the apparent horizon due to grid stretching. To show this, we plotted R_{xyxy} at $t = 100m$ for four different grid resolutions, with 100, 200, 400 and 800 grid points, see figure (14). This clearly shows that the grid resolution has a significant impact on the accuracy of the solution.

6.3. Geodesic slicing

It is well known [23] that for a geodesicly sliced Schwarzschild spacetime (i.e. setting the lapse equal to 1) the throat will collide with the $r = 0$ singularity at coordinate time πm. This provides a simple test – run the code and see when it crashes (its also a curious way to compute π!). We ran the code for 100, 200, 400 and 800 grid points and found that the code crashed within two time steps of $t = 3.14$ (with a time step of 0.01).

6.4. Collapse of the lapse

Beig [24] has shown that for a maximally sliced Schwarzschild spacetime, the lapse at the throat will die exponentially with time,

$$N \sim \beta e^{-\alpha t} + \mathcal{O}\left(e^{-2\alpha t}\right) \quad \text{as } t \to \infty \tag{6.4.1}$$

where

$$\alpha = \frac{4}{3\sqrt{6}} \approx 0.54433 \tag{6.4.2}$$

$$\beta = \frac{4}{3\sqrt{2}} \exp\left(\frac{4\gamma}{3\sqrt{6}}\right) \approx 0.83725 \tag{6.4.3}$$

$$\gamma = \frac{3\sqrt{6}}{4} \ln(54\sqrt{2} - 72) - 2\ln\left(\frac{3\sqrt{3} - 5}{9\sqrt{6} - 22}\right) \approx -0.21815 \tag{6.4.4}$$

See also the earlier works by Estabrook and others [22, 25, 26, 27]. This gives us another test where a plot of $\ln N$ versus t should be a straight line. This we have done in figures (15) and for $t = 10m$ to $t = 100m$ we get a very straight line indeed. Using a standard least squares method we found $\alpha = 0.5474$ and $\beta = 1.011$. Though our estimate of α agrees well with Beig's result, our estimate for β is not so good. This is probably due to a number of factors such as the use of of an inexact outer boundary condition, the problems of grid stretching and numerical error. The numerical error in fitting a straight line could be significant. Notice that for $0 < t < 100m$ the vertical intercept in figure (15) is very small (approximately 0.01) relative to the vertical range (approximately 60). Thus any small errors, either in the data or in fitting the line may produce large *relative* errors in the vertical intercept, namely $\ln \beta$. To demonstrate this point we chose to re-compute α and β by constraining the curve to pass through the data point at $t = 10m$. Thus we applied the least squares method to $\ln N - \ln N(10) = \alpha(t - 10)$ and found $\alpha = 0.5429$ and $\beta = 0.8112$. This is an improvement over our earlier estimates.

At later times, $t = 100m$ to $t = 1000m$ the line does bend slightly. This is not surprising since we know that for these times we have lost accuracy due to grid stretching. Note that at $t = 1000m$ we have $N \sim 10^{-145}$ at the throat – the evolution really has been halted.

6.5. Apparent horizon

An apparent horizon is defined as a closed 2-surface with zero divergence of its outward pointing null vectors [28]. For the Schwarzschild spacetime the apparent horizon must be a 2-sphere whose area must be constant when Lie dragged in the direction of the outward pointing null vectors. Thus

$$0 = \mathcal{L}_u A = \frac{dA}{du} \tag{6.5.1}$$

where A is the area of the 2-sphere and $\partial/\partial u$ is the outward pointing null vector. For our lattice we may put

$$A = kL_{xx}^2 \tag{6.5.2}$$

$$\frac{\partial}{\partial u} = \frac{1}{N}\frac{\partial}{\partial t} + \frac{\partial}{\partial z} \tag{6.5.3}$$

where k is a pure constant, z is the proper distance measured along the radial axis and N is the lapse function. Thus from $0 = dA/du$ we obtain the apparent horizon equation

$$0 = \frac{dL_{xx}}{dz} - L_{xx}K_{xx} \tag{6.5.4}$$

Our aim is to solve this equation for two things i) the location of the apparent horizon and ii) the value of L_{xx}^2 at that location. We do so as follows. First we convert the derivative in L_{xx} into a finite difference approximation using the methods of section 8.8. Then we scan

the grid while monitoring the value of the right hand side of (6.5.4) which we denote by the function $Q(z)$. When we find two successive grid points for which Q changes sign, we stop the scan and then use linear interpolation to predict the true location of the apparent horizon (i.e. z such that $0 = Q$) and any data at that point (e.g. L^2_{xx} and N).

Since there is no gravitational radiation in the Schwarzschild spacetime we know that the area of the apparent horizon must remain constant throughout the evolution. We have plotted $L^2_{xx} = A/k$ in figure (16). For the case of 800 grid points we see that the area varies by less than 4% for the first $100m$ of the evolution. However at later times, around $t = 1000m$, the error has blown out by 700%. This is very large indeed. We do not believe that this is an error in our code but rather a very severe consequence of the loss of resolution due to grid stretching.

Anninos etal. [16] found that for their 1-dimensional code, with a constant $\Delta r = 0.1m$ and an outer boundary at $r = 130m$, that at $t = 25m$ their apparent horizon mass (defined by $M_{ah} = (A/16\pi)^{1/2}$) had grown by about 4% (see their figures 15 and 16). When we repeated their calculations, on their grid but using our equations, we found an error of 3% for the standard scheme and 1% for the grid centred scheme. In a related work, Anninos etal. [15] found that for a grid with 400 points the error in the apparent horizon mass was about 25% at $t = 100m$. For our code, with 400 grid points, we found errors of 12% for the standard scheme and 6% for the grid centred scheme.

We should mention here that setting $A = kL^2_{xx}$ is not strictly correct because the rungs of the ladder are not geodesic segments of the 2-sphere but rather of the surrounding 3-dimensional space. However if the L^2_{xx} are small relative to the area of the apparent horizon then there will be little error in using these legs as approximate geodesics on the apparent horizon.

7. Discussion

The results we have presented are very encouraging. Our most important observation is that the evolution is very stable out to $t = 1000m$. In contrast, the best results using traditional methods (15,16) developed fatal instabilities by about $t = 100$. Thus we are forced to ask the obvious question : What is it about our method that, in this instance, gave us a stable evolution? The features that distinguish our method from traditional methods is that we use a lattice to record the metric, we cover the lattice with a series of Riemann normal frames and we use the Bianchi identities to assist in the computation of the curvatures. It is premature at this stage to identify which, if any, of these ingredients is crucial to the stability, but we can review each of their roles in the method.

Riemann normal coordinates. These were chosen not simply because they allowed us to extract curvatures from the lattice but rather for their relationship with the Einstein equivalence principle. In its full 4-dimensional setting the equivalence principle is equivalent to having the 4-connection vanish in the freely falling frame. Using such frames as a computational tool must surely bring some advantage to the computations. However, we

are actually using the Riemann normal coordinates only for the 3-geometry and thus this argument is not so strong. On the other hand, a zero connection does greatly simplify many of the computations, for example, covariant differentiation reduces to simple partial differentiation. Furthermore, as the source terms in the ADM equations have a different structure to that found in Bernstein, Hobill and Smarr (as a typical example), we can expect that the stability properties may differ from those for traditional methods.

The lattice. This is essential for it provides the structure by which the local Riemann normal frames can be connected together to form a global coordinate atlas for the spacetime. Each pair of adjacent local Riemann normal frames has a non trivial overlap and through the scalar data they share on the lattice the transformation form one frame to another is well defined.

The Bianchi identities. We do not consider the Bianchi identities as central to our method for they were introduced only to overcome a limitation in our highly simplified lattice. We could test their role by redoing our calculations on a more sophisticated lattice. But we should point out that recent work by Christodoulou and Klainerman [29] place great importance on the Bianchi identities in their proof of long term stability for weak initial data.

Another option that may explain the stability is that the method may lack sufficient accuracy, due to dispersion or truncation errors, that the sharp peaks needed to trigger an unstable mode are never resolved. However, our results were always at least as good as those obtained by others (15, 16) which tends to discount this option.

Clearly more work is required by applying this method to other more challenging spacetimes. We shall report on these calculations soon.

8. Appendix

8.1. The Riemann normal frame

It is a simple matter to substitute the coordinates listed in table 1 into the smooth lattice equations (2.4) and the geodesic constraint (3.1.1). This leads directly to the following equations

$$\left(L^{\circ}_{xx}\right)^2 = \left(2u^{\circ}\right)^2 \tag{8.1.1}$$

$$\left(L^{-}_{xx}\right)^2 = \left(2u^{-}\right)^2 - \frac{1}{3}R_{xzxz}\left(2u^{-}v^{-}\right)^2 \tag{8.1.2}$$

$$\left(L^{+}_{xx}\right)^2 = \left(2u^{+}\right)^2 - \frac{1}{3}R_{xzxz}\left(2u^{+}v^{+}\right)^2 \tag{8.1.3}$$

$$\left(L^{-}_{zz}\right)^2 = \left(v^{-}\right)^2 + \left(u^{-} - u^{\circ}\right)^2 - \frac{1}{3}R_{xzxz}\left(u^{\circ}v^{-}\right)^2 \tag{8.1.4}$$

$$\left(L^{+}_{zz}\right)^2 = \left(v^{+}\right)^2 + \left(u^{+} - u^{\circ}\right)^2 - \frac{1}{3}R_{xzxz}\left(u^{\circ}v^{+}\right)^2 \tag{8.1.5}$$

$$0 = \frac{1}{L^{+}_{zz}}\left(u^{\circ} - u^{+} - \frac{1}{3}R_{xzxz}\left(u^{\circ}v^{+}\right)^2\right) + \frac{1}{L^{-}_{zz}}\left(u^{\circ} - u^{-} - \frac{1}{3}R_{xzxz}\left(u^{\circ}v^{-}\right)^2\right) \quad (8.1.6)$$

For a given choice of R_{xzxz} the first five equations can be solved for the coordinates u°, u^{+} etc. The last equation is the geodesic constraint in the form $0 = L^{\circ}_{xx}(\cos\theta^{+} + \cos\theta^{-})$. This equation will constrain the choice of the curvature R_{xzxz}.

Though these equations could be solved using a Newton-Raphson method it would be better if we could find an explicit solution. The simple trick to achieving this hinges on the fact that these equations serve only as an approximation to the true continuum metric and curvatures and are valid only when the domain of the Riemann normal frame is small compared with the curvature lengths scales. Thus it is sufficient to solve the leg length equations by a perturbation expansion around flat space.

Consider the first five equations and let $R_{xzxz} = \mathcal{O}(\epsilon)$ with ϵ taken as our expansion parameter. Then the leading order solution is simply

$$\left(2u^{\circ}\right)_0 = L^{\circ}_{xx} \quad (8.1.7)$$
$$\left(2u^{-}\right)_0 = L^{-}_{xx} \quad (8.1.8)$$
$$\left(2u^{+}\right)_0 = L^{+}_{xx} \quad (8.1.9)$$
$$\left(v^{-}\right)^2_0 = \left(L^{-}_{zz}\right)^2 - \left(u^{-} - u^{\circ}\right)^2_0 \quad (8.1.10)$$
$$\left(v^{+}\right)^2_0 = \left(L^{+}_{zz}\right)^2 - \left(u^{+} - u^{\circ}\right)^2_0 \quad (8.1.11)$$

The next level of approximation is obtained by substituting these back into the above equations and solving once again for the five coordinates. The result is

$$\left(2u^{\circ}\right)_1 = L^{\circ}_{xx} \quad (8.1.12)$$
$$\left(2u^{-}\right)_1 = L^{-}_{xx} + \frac{1}{6}R_{xzxz}L^{-}_{xx}\left(v^{-}\right)^2_0 \quad (8.1.13)$$
$$\left(2u^{+}\right)_1 = L^{+}_{xx} + \frac{1}{6}R_{xzxz}L^{+}_{xx}\left(v^{+}\right)^2_0 \quad (8.1.14)$$
$$\left(v^{-}\right)^2_1 = \left(L^{-}_{zz}\right)^2 - \left(u^{-} - u^{\circ}\right)^2_1 - \frac{1}{3}R_{xzxz}\left(u^{\circ}v^{-}\right)^2_0 \quad (8.1.15)$$
$$\left(v^{+}\right)^2_1 = \left(L^{+}_{zz}\right)^2 - \left(u^{+} - u^{\circ}\right)^2_1 - \frac{1}{3}R_{xzxz}\left(u^{\circ}v^{+}\right)^2_0 \quad (8.1.16)$$

This process could be continued to obtain higher order approximations but that would be a waste of effort as the smooth lattice equations are valid only to linear terms in the curvatures, that is to linear terms in ϵ.

Substituting these approximations into the geodesic constraint and retaining just the terms

linear in ϵ leads to

$$0 = \frac{2}{L^{+}_{zz} + L^{-}_{zz}} \left(\frac{L^{+}_{xx} - L^{\circ}_{xx}}{L^{+}_{zz}} + \frac{L^{-}_{xx} - L^{\circ}_{xx}}{L^{-}_{zz}} \right) + R_{xzxz} L^{\circ}_{xx} \\ - \frac{L^{\circ}_{xx}}{L^{+}_{zz} + L^{-}_{zz}} R_{xzxz} \left(\frac{\left(L^{+}_{xx} - L^{\circ}_{xx}\right)^2}{L^{+}_{zz}} + \frac{\left(L^{-}_{xx} - L^{\circ}_{xx}\right)^2}{L^{-}_{zz}} \right) \tag{8.1.17}$$

This is easily seen to be the finite difference approximation to the differential equation

$$0 = \frac{d^2 L_{xx}}{dz^2} + R_{xzxz} L_{xx} - L_{xx} R_{xzxz} \left(\frac{dL_{xx}}{dz} \right)^2 \tag{8.1.18}$$

which we recognise, apart from the last term, to be the standard geodesic deviation equation applied to the two radial geodesics. By making the simple change of scale $L_{xx} \to \lambda L_{xx}$ we can see that for $\lambda << 1$ (i.e. for very short leg lengths) the last term is insignificant compared to the remaining terms (at a fixed position on the radial axis). This is to be expected since for the two radial geodesics to be nearly parallel everywhere we must have $dL_{xx}/dz << 1$.

Upon deleting this term from the discrete equations we obtain

$$0 = \frac{2}{L^{+}_{zz} + L^{-}_{zz}} \left(\frac{L^{+}_{xx} - L^{\circ}_{xx}}{L^{+}_{zz}} + \frac{L^{-}_{xx} - L^{\circ}_{xx}}{L^{-}_{zz}} \right) + R_{xzxz} L^{\circ}_{xx} \tag{3.2.1}$$

as our basic equation from which we can compute the curvature R_{xzxz}.

Incidentally this requirement that the two radial geodesics be nearly parallel everywhere also shows that $\left(L^{-}_{zz}\right)^2 >> \left(u^{-} - u^{\circ}\right)^2_0$ and thus to leading order $\left(v^{-}\right)_0 = -\left(L^{-}_{zz}\right)$. Proceeding in this fashion we find the following estimates for the coordinates.

$$\left(2u^{\circ}\right)_1 = L^{\circ}_{xx} \tag{8.1.19}$$

$$\left(2u^{-}\right)_1 = L^{-}_{xx} + \frac{1}{6} R_{xzxz} L^{-}_{xx} \left(L^{-}_{zz}\right)^2 \tag{8.1.20}$$

$$\left(2u^{+}\right)_1 = L^{+}_{xx} + \frac{1}{6} R_{xzxz} L^{+}_{xx} \left(L^{+}_{zz}\right)^2 \tag{8.1.21}$$

$$\left(v^{-}\right)_1 = L^{-}_{zz} - \frac{1}{24} R_{xzxz} L^{-}_{zz} \left(L^{\circ}_{xx}\right)^2 \tag{8.1.22}$$

$$\left(v^{+}\right)_1 = L^{+}_{zz} - \frac{1}{24} R_{xzxz} L^{+}_{zz} \left(L^{\circ}_{xx}\right)^2 \tag{8.1.23}$$

These estimates will be of use later in Appendix 8.2.

8.2. The 1+1 ADM evolution equations

In the paper by Brewin [12] the 3+1 ADM evolution equations for a lattice where given as

$$\frac{d^2 L_{ij}^2}{dt^2} = -2\left(\frac{d}{dt}(NK_{\mu\nu})\right)\Delta x_{ij}^{\mu}\Delta x_{ij}^{\nu} + Q_{ij} \tag{8.2.1}$$

where Q_{ij} represented the terms involving the shift and drift vectors. We shall immediately set $Q_{ij} = 0$ since this corresponds to our lattice which has zero shift and drift.

For many reasons (in particular, for ease of numerical integration) it is customary to express the evolution equations as a system of first order equations. This will be the main focus of this section.

In [12] two important coordinate frames were used. The first was the Riemann normal frame for a given computational cell in one Cauchy surface Σ_0. These coordinates were denoted by x^{μ}. Some of these coordinates could be freely chosen (by aligning the coordinate axes) on some of the vertices of the cell (in particular, at the origin of the cell). For the remaining vertices the coordinates must be computed during the solution of the lattice equations

$$L_{ij}^2 = g_{\mu\nu}\Delta x_{ij}^{\mu}\Delta x_{ij}^{\nu} - \frac{1}{3}R_{\mu\alpha\nu\beta}x_i^{\mu}x_i^{\nu}x_j^{\alpha}x_j^{\beta} \tag{8.2.2}$$

Since the leg lengths are expected to be functions of time we must also expect that in the Riemann normal frame the vertex coordinates x_i^{μ} will also be functions of time. Thus in this frame we may choose the shift and drift to be zero at the origin of the cell but must accept non-zero values elsewhere.

The second frame used in [12] was not a Riemann normal frame but one in which the shift and drift vectors where set to zero everywhere. These coordinates were denoted by x''^{μ}. On the initial Cauchy surface the two coordinate frames are identical, $x^{\mu} = x''^{\mu}$ on Σ_0, but for future times the coordinates will differ. This establishes a time dependent transformation between the two coordinate frames.

Consider for the moment the shadow frame with coordinates x''^{μ}. For the case of zero shift and drift the standard definition of the extrinsic curvature is

$$\frac{dg''_{\mu\nu}}{dt} = -2NK''_{\mu\nu} \tag{8.2.3}$$

The leg lengths can be estimated from

$$L_{ij}^2 = g''_{\mu\nu}\Delta x_{ij}^{''\mu}\Delta x_{ij}^{''\nu} \tag{8.2.4}$$

But in this frame $0 = dx_i^{''\mu}/dt$ and thus we have

$$\frac{dL_{ij}^2}{dt} = -2NK''_{\mu\nu}\Delta x_{ij}^{''\mu}\Delta x_{ij}^{''\nu} \tag{8.2.5}$$

which when evaluated on Σ_0, where the two frames coincide, we have

$$\frac{dL_{ij}^2}{dt} = -2NK_{\mu\nu}\Delta x_{ij}^{\mu}\Delta x_{ij}^{\nu} \tag{4.1.1}$$

Now consider the time derivative of this last pair of equations. These may be written as

$$\frac{d^2L_{ij}^2}{dt^2} = -2N\frac{dK''_{\mu\nu}}{dt}\Delta x''^{\mu}_{ij}\Delta x''^{\nu}_{ij} - 2\frac{dN}{dt}K''_{\mu\nu}\Delta x''^{\mu}_{ij}\Delta x''^{\nu}_{ij} \tag{8.2.6}$$

and

$$\frac{d^2L_{ij}^2}{dt^2} = -2N\frac{d}{dt}\left(K_{\mu\nu}\Delta x_{ij}^{\mu}\Delta x_{ij}^{\nu}\right) - 2\frac{dN}{dt}K_{\mu\nu}\Delta x_{ij}^{\mu}\Delta x_{ij}^{\nu} \tag{8.2.7}$$

which if we now combine with the standard ADM equation

$$\frac{dK''_{\mu\nu}}{dt} = -N_{|\mu\nu} + N\left(R_{\mu\nu} + KK_{\mu\nu} - 2K_{\mu\alpha}K^{\alpha}_{\nu}\right) \tag{8.2.8}$$

leads directly to

$$\frac{d}{dt}\left(K_{\mu\nu}\Delta x_{ij}^{\mu}\Delta x_{ij}^{\nu}\right) = \left(-N_{,\mu\nu} + N\left(R_{\mu\nu} + KK_{\mu\nu} - 2K_{\mu\alpha}K^{\alpha}_{\nu}\right)\right)\Delta x_{ij}^{\mu}\Delta x_{ij}^{\nu} \tag{4.1.2}$$

on Σ_0. We have written $N_{,\mu\nu}$ as opposed to $N_{|\mu\nu}$ since in the Riemann normal frame the connection vanishes at the origin and thus $N_{,\mu\nu} = N_{|\mu\nu}$ on the central vertex of the computational cell.

This completes our stated aim – to derive a pair of first order evolution equations – (4.1.1) and (4.1.2). These will now be applied to the lattice. To do so first requires equations (2.4,2.5) to be solved for the coordinates x^{μ} for each vertex in the computational cell. This was done in section 8.1 and lead to equations (8.1.19–8.1.23). Substituting these in (4.1.1,4.1.2) and retaining only the leading order terms we find

$$\frac{dL_{xx}}{dt} = -NK_{xx}L_{xx} \tag{4.1.3}$$

$$\frac{dL_{zz}}{dt} = -NK_{zz}L_{zz} \tag{4.1.4}$$

$$\frac{dK_{xx}}{dt} = -N_{,xx} + N\left(R_{xx} + KK_{xx}\right) \tag{4.1.5}$$

$$\frac{dK_{zz}}{dt} = -N_{,zz} + N\left(R_{zz} + KK_{zz}\right) \tag{4.1.6}$$

8.3. The ADM evolution equations : An alternative derivation

There is another way in which all of the above equations can be easily developed. The idea is to begin with the usual ansatz for a spherically symmetric space such as

$$ds^2 = -N^2(r,t)dt^2 + A^2(r,t)dr^2 + B(r,t)^2(d\theta^2 + \sin^2\theta d\phi^2) \tag{8.3.1}$$

and to build a lattice in the $\theta = \pi/2$ plane by assigning leg lengths according to

$$L_{xx} = B\Delta\phi \tag{8.3.2}$$
$$L_{zz} = A\Delta r \tag{8.3.3}$$

The functions A and B would be evaluated at the centre of each leg while Δr and $\Delta\phi$ would be chosen as some suitably small numbers.

The standard ADM equations, for a metric with zero shift, are

$$\frac{dg_{\mu\nu}}{dt} = -2NK_{\mu\nu} \tag{8.3.4}$$
$$\frac{dK_{\mu\nu}}{dt} = -N_{|\mu\nu} + N\left(R_{\mu\nu} + KK_{\mu\nu} - 2K_{\mu\alpha}K^{\alpha}{}_{\nu}\right) \tag{8.3.5}$$

We now ask the simple question: What form do these equations take when applied to a lattice? The answer is also simple. Since there is no shift vector, the coordinates of each vertex remain constant throughout the evolution, thus $0 = d\Delta x^{\mu}_{ij}/dt$ and we therefore have

$$\frac{d}{dt}\left(g_{\mu\nu}\Delta x^{\mu}_{ij}\Delta x^{\nu}_{ij}\right) = -2NK_{\mu\nu}\Delta x^{\mu}_{ij}\Delta x^{\nu}_{ij} \tag{8.3.6}$$
$$\frac{d}{dt}\left(K_{\mu\nu}\Delta x^{\mu}_{ij}\Delta x^{\nu}_{ij}\right) = \left(-N_{|\mu\nu} + N\left(R_{\mu\nu} + KK_{\mu\nu} - 2K_{\mu\alpha}K^{\alpha}{}_{\nu}\right)\right)\Delta x^{\mu}_{ij}\Delta x^{\nu}_{ij} \tag{8.3.7}$$

These differ from the smooth lattice equations (4.1.3–4.1.6) only in how the terms $N_{|\mu\nu}$ and $R_{\mu\alpha\nu\beta}$ are computed. It is easy to show that for the above metric

$$N_{|rr} = N_{,rr} - \frac{1}{A}A_{,r}N_{,r} \tag{8.3.8}$$
$$N_{|\phi\phi} = N_{,\phi\phi} + \frac{B}{A^2}B_{,r}N_{,r} \tag{8.3.9}$$
$$R_{r\phi r\phi} = \frac{B}{A}\left(A_{,r}B_{,r} - AB_{,rr}\right) \tag{8.3.10}$$
$$R_{\theta\phi\theta\phi} = \left(\frac{B}{A}\right)^2\left(A^2 - (B_{,r})^2\right) \tag{8.3.11}$$
$$0 = 2B_{,r}R_{r\phi r\phi} - BA^2\left(\frac{R_{\theta\phi\theta\phi}}{B^2}\right)_{,r} \tag{8.3.12}$$

These equations can be adapted to the lattice by making a coordinate transformation into a local Riemann normal frame

$$dz = Adr \tag{8.3.13}$$

$$dx = Bd\phi \tag{8.3.14}$$

$$N_{,zz} = \frac{1}{A^2} N_{|rr} \tag{8.3.15}$$

$$N_{,xx} = \frac{1}{B^2} N_{|\phi\phi} \tag{8.3.16}$$

$$R_{xzxz} = \frac{1}{A^2 B^2} R_{r\phi r\phi} \tag{8.3.17}$$

$$R_{xyxy} = \frac{1}{B^4} R_{\theta\phi\theta\phi} \tag{8.3.18}$$

and then eliminating, where possible, A and B in favour of L_{xx} and L_{zz}. This leads directly to the smooth lattice equations (3.2.1, 3.2.3, 4.1.7, 4.1.8). The exception is the equation for $R_{\theta\phi\theta\phi}$ for which there is no direct counterpart in the smooth lattice equations. For this quantity we find

$$R_{xyxy} = \frac{1}{L_{xx}^2} \left(\Delta\phi^2 - \left(\frac{dL_{xx}}{dz} \right)^2 \right) \tag{8.3.19}$$

This equation can not be used on this lattice for two reasons. First, there is no clear method for determining the parameter $\Delta\phi$ from the lattice data L_{xx} and L_{zz}. Second, this equation simply does not arise as a consequence of the basic smooth lattice equations (2.4, 2.5). This problem could be overcome by employing a different lattice. For example, if we chose a lattice in which each 2-sphere was fully triangulated then we could reasonably expect that both curvatures could be computed from the smooth lattice equations without reference to the Bianchi identities. On such a lattice we should also be able to compute $\Delta\phi$.

This alternative derivation is useful not only in giving us confidence that we have the correct lattice equations but it also gives us a technique for quickly adapting a continuum equation directly to the lattice. Indeed we could well have chosen this as the primary method by which to develop our equations.

8.4. Covariant differentiation

Since the connection vanishes in Riemann Normal Coordinates we have, for any vector field, that

$$v^{\mu}{}_{;\nu} = v^{\mu}{}_{,\nu} \tag{8.4.1}$$

at the origin of the RNC cell.

There are probably many ways in which the partial derivatives could be evaluated, however, in this section we shall focus on a method based on coordinate transformations and finite differences.

The basis of our approach is to import values of the vector field from neighbouring RNC cells, by simple coordinate transformations such as rotations and translations, and to then use this data in a finite difference approximation. This is exactly the same as parallel transport since, once again, the connection vanishes, and thus to leading order we can construct the transformations as if we were in flat space.

We will demonstrate this approach for a spherically symmetric 3-geometry. Consider a typical RNC cell with its axes oriented as per figure 3. This cell will be denoted by $\sigma^{\mathtt{o}}$ while four of its six immediate neighbours will be denoted by $\sigma^{\mathtt{l}}$, $\sigma^{\mathtt{r}}$, being the left and right neighbours of σ^o, and $\sigma^{\mathtt{+}}$, $\sigma^{\mathtt{-}}$ being the cells above and below $\sigma^{\mathtt{o}}$ along the radial axis. The remaining to cells lie along the y-axis relative to $\sigma^{\mathtt{o}}$ and we will have no need of these cells in the following calculations. We will use these superscripts to denote quantities which are defined relative to the cell with the same superscript.

Suppose we have a spherically symmetric vector field v^μ. Then each cell on a 2-sphere will share exactly the same values for v^μ in their respective local RNC frames, that is

$$v^{\mu\mathtt{l}} = v^{\mu\mathtt{r}} = v^{\mu\mathtt{o}} \tag{8.4.2}$$

for each i, j. We will now import these values into the central cell σ^o. Consider first the cells $\sigma^{\mathtt{o}}$ and $\sigma^{\mathtt{r}}$. The RNC coordinates of these frames are related by a rotation (to align the directions of their axes) and a translation (to align their origins) which we will write as

$$x^{\mu\mathtt{r}} = A^\mu{}_\nu x^{\mu\mathtt{o}} + B^\mu \tag{8.4.3}$$

The situation is depicted in figure 4.

The components $A^\mu{}_\nu$ can be assembled into a rotation matrix

$$[A^\mu{}_\nu] = \begin{bmatrix} \cos\Delta\theta & 0 & \sin\Delta\theta \\ 0 & 1 & 0 \\ -\sin\Delta\theta & 0 & \cos\Delta\theta \end{bmatrix} \approx \mathrm{I} + \Delta\theta \begin{bmatrix} 0 & 0 & 1 \\ 0 & 0 & 0 \\ -1 & 0 & 0 \end{bmatrix} \tag{8.4.4}$$

where $\Delta\theta$ is a (small) angle of rotation and where μ is taken as the row index. The approximation that $\Delta\theta$ is small is imposed so that the we have an accurate approximation to the continuum geometry. By inspection of figure 3 we see that $\Delta\theta = \Delta L_{xx}/\Delta z$.

Using the standard tensor transformation laws we find that the values of $v^{\mu\mathtt{r}}$ in the RNC frame of $\sigma^{\mathtt{o}}$ to be

$$v'^{\mu\mathtt{r}} = \frac{\partial x^{\mu\mathtt{r}}}{\partial x^{\nu\mathtt{o}}} v^{\nu\mathtt{r}} = A^\mu{}_\nu v^{\nu\mathtt{o}} \tag{8.4.5}$$

Thus for cells $\sigma^{\mathtt{l}}$ and $\sigma^{\mathtt{r}}$ we find

$$v'^{x\mathtt{r}} = v^{x\mathtt{o}} + \Delta\theta v^{z\mathtt{o}} \tag{8.4.6}$$

$$v'^{y\mathtt{r}} = v^{y\mathtt{o}} \tag{8.4.7}$$

$$v'^{z\mathtt{r}} = v^{z\mathtt{o}} - \Delta\theta v^{x\mathtt{o}} \tag{8.4.8}$$

$$v'^{x\mathtt{l}} = v^{x\mathtt{o}} - \Delta\theta v^{z\mathtt{o}} \tag{8.4.9}$$

$$v'^{y\mathtt{l}} = v^{y\mathtt{o}} \tag{8.4.10}$$

$$v'^{z\mathtt{l}} = v^{z\mathtt{o}} + \Delta\theta v^{x\mathtt{o}} \tag{8.4.11}$$

Since these two cells reside on opposite sides of the $yz-$plane we can use the above to form a centred finite difference approximation for $v^{\mu}{}_{,x}$ at the origin of $\sigma^{\mathtt{o}}$, namely

$$v^{\mu}{}_{,x} = \frac{v^{\mu\mathtt{r}} - v^{\mu\mathtt{l}}}{\Delta x} \tag{8.4.12}$$

where Δx is, to leading order, the distance between the origins of cells $\sigma^{\mathtt{r}}$ and $\sigma^{\mathtt{l}}$. This is easily seen to be $2L_{xx}$, leading to

$$v^{x}{}_{;x} = v^{x}{}_{,x} = \quad \frac{1}{L_{xx}}\frac{\Delta L_{xx}}{\Delta z} v^{z\mathtt{o}} \tag{8.4.13}$$

$$v^{y}{}_{;x} = v^{y}{}_{,x} = 0 \tag{8.4.14}$$

$$v^{z}{}_{;x} = v^{z}{}_{,x} = -\frac{1}{L_{xx}}\frac{\Delta L_{xx}}{\Delta z} v^{x\mathtt{o}} \tag{8.4.15}$$

The same idea can be applied to derivatives in the y direction, leading to

$$v^{x}{}_{;y} = v^{x}{}_{,y} = 0 \tag{8.4.16}$$

$$v^{y}{}_{;y} = v^{y}{}_{,y} = \quad \frac{1}{L_{xx}}\frac{\Delta L_{xx}}{\Delta z} v^{z\mathtt{o}} \tag{8.4.17}$$

$$v^{z}{}_{;y} = v^{z}{}_{,y} = -\frac{1}{L_{xx}}\frac{\Delta L_{xx}}{\Delta z} v^{y\mathtt{o}} \tag{8.4.18}$$

which clearly could also have been derived by simple symmetry arguments. The $z-$derivatives are very easy to calculate. Since the RNC frames of the three cells $\sigma^{\mathtt{o}}, \sigma^{\mathtt{-}}$ and $\sigma^{\mathtt{+}}$ are related by simple translations along the z-axis, the coordinate transformations are trivial and lead directly to

$$v^{x}{}_{;z} = v^{x}{}_{,z} = \frac{\Delta v^{x}}{\Delta z} \tag{8.4.19}$$

$$v^{y}{}_{;z} = v^{y}{}_{,z} = \frac{\Delta v^{y}}{\Delta z} \tag{8.4.20}$$

$$v^{z}{}_{;z} = v^{z}{}_{,z} = \frac{\Delta v^{z}}{\Delta z} \tag{8.4.21}$$

It is useful to make one small change to the above. We will replace the finite difference approximations by their continuum limits (i.e. $\Delta \mapsto d$) to simplify the presentations in the following sections.

8.5. The Laplacian

Let ϕ be a function which is constant on each 2-sphere of a spherically symmetric space. If we put $v^\mu = \phi^{;\mu}$ then at the origin of each RNC cell we have $v^\mu = \phi_{,\mu}$ since $g_{\mu\nu} = \mathrm{diag}(1,1,1)$ and $0 = \Gamma^\mu{}_{\alpha\beta}$ at the origin of each RNC frame. Since ϕ is constant on each 2-sphere, we must have,

$$\phi_{,x} = 0, \qquad \phi_{,y} = 0, \qquad \phi_{,z} = \frac{d\phi}{dz} \tag{8.5.1}$$

on the $z-$axis. Using this and the results of the previous section we find that, on the $z-$axis

$$\phi_{,xy} = v^x{}_{,y} = 0 \tag{8.5.2}$$

$$\phi_{,xz} = v^x{}_{,z} = \frac{dv^x}{dz} = 0 \tag{8.5.3}$$

$$\phi_{,yz} = v^y{}_{,z} = \frac{dv^y}{dz} = 0 \tag{8.5.4}$$

$$\phi_{,xx} = v^x{}_{,x} = \frac{1}{L_{xx}}\frac{dL_{xx}}{dz}\frac{d\phi}{dz} \tag{8.5.5}$$

$$\phi_{,yy} = v^y{}_{,y} = \frac{1}{L_{xx}}\frac{dL_{xx}}{dz}\frac{d\phi}{dz} \tag{8.5.6}$$

$$\phi_{,zz} = v^z{}_{,z} = \frac{d^2\phi}{dz^2} \tag{8.5.7}$$

and thus

$$\nabla^2\phi = \frac{d^2\phi}{dz^2} + \frac{2}{L_{xx}}\frac{dL_{xx}}{dz}\frac{d\phi}{dz} \tag{8.5.8}$$

It is easy to see that this leads to the correct Laplacian for flat space (i.e. put $L_{xx} = r\Delta\theta$ and $r = z$ where r is the usual radial coordinate and z is the proper distance measured along the radial axis).

8.6. The ADM Constraints

The Hamiltonian constraint

$$0 = R + K^2 - K^{\mu\nu}K_{\mu\nu} \tag{4.2.1}$$

can be evaluated directly on the lattice as each term on the right hand side is known at each vertex of the lattice. Furthermore, since the lattice is spherically symmetric the only terms which survive are those that contain $R_{xyxy}, R_{xzxz}, K_{xx}$ and K_{zz}. This leads to

$$0 = R_{xyxy} + 2R_{xzxz} + K_{xx}^2 + 2K_{xx}K_{zz} \tag{4.2.3}$$

The standard form of the ADM momentum constraints are

$$0 = K_{|\mu} - K_\mu{}^\nu{}_{|\nu} \tag{8.6.1}$$

where $K = K^{\mu}{}_{\mu}$. These equations require more care as they contain covariant derivatives. At the origin of a RNC frame we have $g_{\mu\nu} = \mathrm{diag}(1,1,1)$ and $0 = \Gamma^{\mu}_{\alpha\beta}$, and thus the constraints may be reduced to

$$0 = K_{,\mu} - K_{\mu}{}^{\nu}{}_{,\nu} \tag{8.6.2}$$

Each of the partial derivatives can be evaluated using the methods of the previous section (though modified for use on a two index tensor). The results are

$$K_{,x} = K_{,y} = 0 \tag{8.6.3}$$

$$K_{,z} = \frac{dK_{xx}}{dz} + \frac{dK_{yy}}{dz} + \frac{dK_{zz}}{dz} \tag{8.6.4}$$

$$K_x{}^{\mu}{}_{,\mu} = K_y{}^{\mu}{}_{,\mu} = 0 \tag{8.6.5}$$

$$K_z{}^{\mu}{}_{,\mu} = \frac{1}{L_{xx}}\frac{dL_{xx}}{dz}\left(2K_{zz} - K_{xx} - K_{yy}\right) + \frac{dK_{zz}}{dz} \tag{8.6.6}$$

One also finds that terms such as $K_{xz,x} \neq 0$ even though $K_{xz} = 0$ at the origin of each RNC cell. This fact has been used in the above results.

The only non-trivial momentum equation is that for $\mu = z$ and this leads to

$$0 = \frac{d\left(L_{xx}K_{xx}\right)}{dz} - K_{zz}\frac{dL_{xx}}{dz} \tag{4.2.4}$$

where we have used the fact that $K_{xx} = K_{yy}$ in our RNC frame.

8.7. Bianchi Identities

The Bianchi identities in a RNC frame are just

$$0 = R_{\mu\nu\alpha\beta,\rho} + R_{\mu\nu\beta\rho,\alpha} + R_{\mu\nu\rho\alpha,\beta} \tag{8.7.1}$$

In a spherically symmetric space there is only one non-trivial Bianchi identity, namely,

$$0 = R_{xyxy,z} + R_{xyyz,x} + R_{xyzx,y} \tag{8.7.2}$$

The only non-zero components of the Riemann tensor at the origin of a RNC cell are $R_{xzxz} = R_{yzyz}$ and R_{xyxy} (and others obtained by standard symmetries in the indicies). However, like the calculations above for the momentum constraints, we find that many terms including $R_{xyyz,x}$ and $R_{xyzx,y}$ are not zero. This fact is a simple consequence of the mixing that occurs amongst the non-zero $R_{\mu\nu\alpha\beta}$ brought about by the rotation matrices. Rather than list all of the non-zero derivatives we shall list only those that we need for the above Bianchi identity. They are

$$R_{xyxy,z} = \frac{dR_{xyxy}}{dz} \tag{8.7.3}$$

$$R_{xyyz,x} = \frac{1}{L_{xx}} \frac{dL_{xx}}{dz} \left(R_{xzxz} - R_{xyxy} \right) \tag{8.7.4}$$

$$R_{xyxz,y} = \frac{1}{L_{xx}} \frac{dL_{xx}}{dz} \left(R_{xzxz} - R_{xyxy} \right) \tag{8.7.5}$$

which when substituted into the above equation leads to

$$0 = \frac{d\left(L_{xx}^2 R_{xyxy}\right)}{dz} - R_{xzxz} \frac{dL_{xx}^2}{dz} \tag{3.2.4}$$

8.8. Non-uniform finite differences

By applying standard Taylor series expansions to a smooth function $f(z)$ it is easy to derive the following second order accurate finite difference approximations

$$\frac{df}{dz} = \frac{1}{L_{zz}^{+} + L_{zz}^{-}} \left(L_{zz}^{-} \left(\frac{f^{+} - f^{\circ}}{L_{zz}^{+}} \right) + L_{zz}^{+} \left(\frac{f^{\circ} - f^{-}}{L_{zz}^{-}} \right) \right) \tag{8.8.1}$$

$$\frac{d^2 f}{dz^2} = \frac{2}{L_{zz}^{+} + L_{zz}^{-}} \left(\frac{f^{+} - f^{\circ}}{L_{zz}^{+}} + \frac{f^{-} - f^{\circ}}{L_{zz}^{-}} \right) \tag{8.8.2}$$

for a non-uniform lattice (where $L_{zz}^{+} \neq L_{zz}^{-}$ are the lattice spacings). Centred finite differences are not appropriate for two simple reasons. First, we chose our initial data L_{zz} to be non-uniform. Second, even if we did choose an initially uniform lattice, the subsequent dynamics ($dL_{zz}/dt \neq 0$) would immediately produce a non-uniform lattice.

These approximations are used at various places in the text (e.g. for dL_{xx}/dz and d^2N/dz^2).

The only exception to the above was in the discretisation of the Bianchi identities. This equation was approximated at the centre of the radial struts by a forward finite difference operator $df/dz = (f^{+} - f^{\circ})/L_{zz}^{+}$ and by setting $R_{xzxz} = (R_{xzxz}^{+} + R_{xzxz}^{\circ})/2$.

9. References

[1] Alcubierre, M., Allen, G., Brugmann, B., Seidel, E. and Suen, W-M. *Towards and understanding of stability properties of the 3+1 evolution equations in general relativity.* Phys.Rev.D. Vol.62(2000) p.124011

[2] Alcubierre, M., Brugamnn, B., Dramlitsch, T., Font, J.A., Papadopoulos, P., Seidel, E., Stegioulas, N. and Takahashi, R., *Towards a stable numerical evolution of strongly gravitating systems in general relativity : The conformal treatments.* Phys.Rev.D. Vol.62(2000) p.044034

[3] Baumgarte, T.W. and Shapiro, S.L. *Numerical integration of Einstein's field equations.* Phys.Rev.D. Vol.59(1999) p.024007

[**4**] Kelly, B., Laguna, P., Lockitch, K., Pullin, J., Schnetter, E., Shoemaker, D. and Tiglio, M. *A cure for unstable numerical evolutions of single black holes: adjusting the standard ADM equations.* `gr-qc/0103099`

[**5**] Scheel, M.A., Baumgarte, T.W, Cook, G.B., Shapiro, S.L., and Teukolsky, S.A. *Treating instabilities in a hyperbolic formulation of Einstein's equations.* Phys.Rev.D. Vol.58(1998). p.044020.

[**6**] Shibata, M. and Nakamura, T. *Evolution of three-dimensional gravitational waves : Harmonic slicing case.* Phys.Rev.D. Vol.52(1995) pp.5428-5444

[**7**] Gen Yoneda and Hisa-aki Shinkai. *Constraint propagation in the family of ADM systems.* `gr-qc/0103032`

[**8**] Reula, O.A. *Hyperbolic methods for Einstein's equations.* Living Reviews in Relativity `http://www.livingreviews.org/`

[**9**] Alcubierre, M., Brugmann, B., Miller, M. and Suen, W-M. *A conformal hyperbolic formulation of the Einstein equations.* Phys.Rev.D. Vol.60(1999) p.064017

[**10**] Scheel, M.A., Baumgarte, T.W, Cook, G.B., Shapiro, S.L., and Teukolsky, S.A. *Numerical evolution of black holes with a hyperbolic formulation of general relativity.* Phys.Rev.D. Vol.56(1997) pp.6320-6335.

[**11**] Brewin, L.C. *Riemann normal coordinates, smooth lattices and numerical relativity.* Class.Q.Gravity. Vol.15(1998) pp.3085-3120.

[**12**] Brewin, L.C. *A 3+1 ADM formulation for smooth lattice general relativity.* Class.Q.Gravity. Vol.15(1998) pp.2427-2449.

[**13**] Bernstein, D., Hobill, D., Seidel, E., Smarr, L. and Towns, J. *Numerically generated axisymmetric black hole spacetime: Numerical methods and code tests.* Phys.Rev.D. Vol.50(1994) pp.5000-5024.

[**14**] Bernstein, D., Hobill, D. and Smarr, L. *Black hole spacetimes : testing numerical relativity. Frontiers in numerical relativity.* eds. Evans, Finn and Hobill. CUP. (1989).

[**15**] Anninos, P., Daues, G., Masso, J., Seidel, E. and Suen, W-M. *Horizon boundary condition for black hole spacetimes.* Phys.Rev.D. Vol.51(1995) pp.5562-5578.

[**16**] Anninos, P., Camarda, K., Masso, J., Seidel, E., Seun, W-M. and Towns, J. *Three dimensional numerical relativity : the evolution of black holes.* Phys.Rev.D. Vol.52(1995) pp.2059-2082.

[**17**] Brewin, L.C. *Riemann normal coordinates.* Preprint. `http://www.maths.monash.edu.au/~leo/preprints/rnc.ps.gz`

[**18**] Petrov, A.Z. *Einstein Spaces. (Chp.1 sec.7)* Pergamon Press, Oxford. 1969

[**19**] Eisenhart, L.P. *Riemannian geometry.(Sec.18 and App.3)* Princeton University Press, Princeton 1926

[**20**] Misner, C.W, Thorne, K. and Wheeler, J.A. *Gravitation (pp.285-287)* W.H. Freeman. San Francisco. 1973.

[**21**] Berger, M.J. and Oliger, J. *Adaptive mesh refinement for hyperbolic partial differential equations.* J.Comp.Physics. Vol.53(1984) pp.484-512.

[**22**] Estabrook, F., Wahlquist, H., Christensen, S., DeWitt, B., Smarr, L. and Tsiang, E. *Maximally slicing a black hole.* Phys.Rev.D. Vol.7(1973) pp.2814-2817.

[**23**] Misner, C.W, Thorne, K. and Wheeler, J.A. *Gravitation* W.H. Freeman. San Francisco. 1973.

[**24**] Beig, R. *The maximal slicing of a Schwarzschild black hole.* Ann. Phys. Vol.11(2000) pp.507-510.

[**25**] Petrich, L.I, Shapiro, S.L and Teukolsky, S.A. *Oppenheimer-Snyder collapse with maximal time slicing and isotropic coordinates.* Phys.Rev.D. Vol.31(1985) pp.2459-2469.

[**26**] Reinhart, B.L. *Maximal foliations of extneded Schwarzschild space.* J.Maths.Phys. Vol.14(1973) p.719.

[**27**] Smarr, L. and York, J.W. *Kinematical conditions in the construction of spacetime.* Phys.Rev.D. Vol.17(1978) pp.2529-2551.

[**28**] Hawking, S.W. and Ellis, G.F.R. *The large scale structure of space-time.* CUP. 1973.

[**29**] Christodoulou, D. and Klainerman, S. *The global nonlinear stability of the Minkowski Space.* Princeton Universiy Press, Princeton, USA. 1993.

Figure captions

Figure 1. An embedding diagram for a 2-dimensional slice of the spherically symmetric 3-geometry of a Schwarzschild black hole. The lattice is constructed as a ladder, with one end on the throat and the other in the weak field region of the black hole. The two radial edges of the ladder are radial geodesics, while each rung is a geodesic segment of the full 3-metric. Thus each rung is not confined to the 2-spheres (except at the throat).

Figure 2. The ladder on which the numerical solution was built. Successive computational cells overlap by sharing two successive rungs of the ladder. In this diagram there are just three computational cells. The production runs employed 800 rungs and had an outer boundary set at approximately $r = 200M$.

Figure 3. A typical computational cell. The coordinate frame has been oriented so that the z-axis points in the usual radial direction while the origin has been located so that the z coordinate of vertices (1) and (2) equals zero. The $y-$axis points directly into the page and thus it has been suppressed.

Figure 4. The three neighbouring computational cells used in applying the Binachi identities. For simplicity we have not drawn the middle rungs in each cell and we have drawn each geodesic segment as a straight line. Once again the y-axis has been suppressed.

Figure 5–13. These figures show the evolution of the basic lattice data for $t = 10m$ to $t = 100m$ in steps of $10m$ and also from $t = 100m$ to $t = 1000m$ in steps of $100m$. All of the figures display a smooth evolution with no signs of any instabilities. In each of these figures we can clearly see the stretching that occurs in the grid. On each curve we have used a diamond to mark the location of the apparent horizon. In many of the figures for $0 < t < 100m$ we can clearly see the loss of resolution brought on by the grid stretching (e.g. the fall off in the plateau of K_{xx} and in the decay in the sharp peak of K_{zz}). These effects are much more pronounced in the long term evolution, $100m < t < 1000m$. Note that at these late times the radial legs near the apparent horizon have been stretched by almost a factor of 100 while the rungs have been shrunk be a factor of approximately 100. This is a severe change in shape of the grid and so its not surprising that the accuracy has been lost. Each of the plots in figures 5–13 were produced using the grid centred scheme on a Bernstein, Hobill and Smarr grid with 800 grid points. The plots for $0 < t < 100m$ were restricted to a proper distance of $100m$ simply to better display the changes in the grid. At $t = 100m$ the grid extends out to a proper distance of over $265m$.

Figure 14. This displays the curvature term R_{xyxy} at $t = 100m$ for four different resolutions of 100, 200, 400 and 800 grid points. This clearly shows that the ability to maintain a flat plateau behind the horizon is compromised when there is a loss of resolution near the apparent horizon.

Figure 15. This shows the exponential collapse of the lapse at the throat. The work of Beig [24] shows that $N(r = 0) \sim e^{kt}$ thus a plot of $\ln N$ versus t should be a straight line. For $t = 0$ to $t = 100m$ the line is very straight, while for longer times a slight bend does occur. The lapse at the throat at $t = 100m$ is approximately 3.4×10^{-23} while at $t = 1000m$ is the lapse is of the order of 10^{-145}.

Figure 16. The size of the apparent horizon from $t = 0$ to $t = 100m$ for four different resolutions of 100, 200, 400 and 800 grid points.

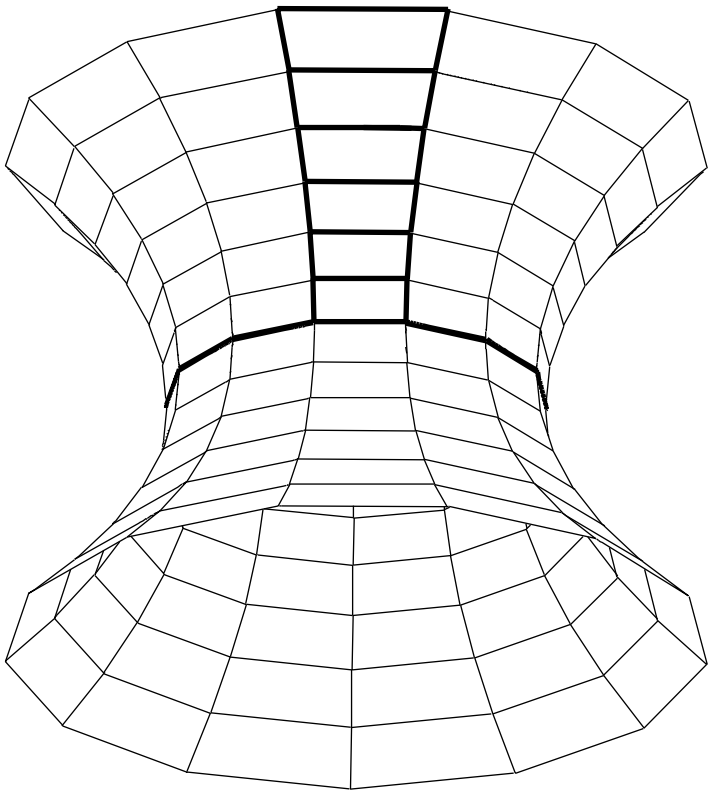

Figure 1. The embedding diagram.

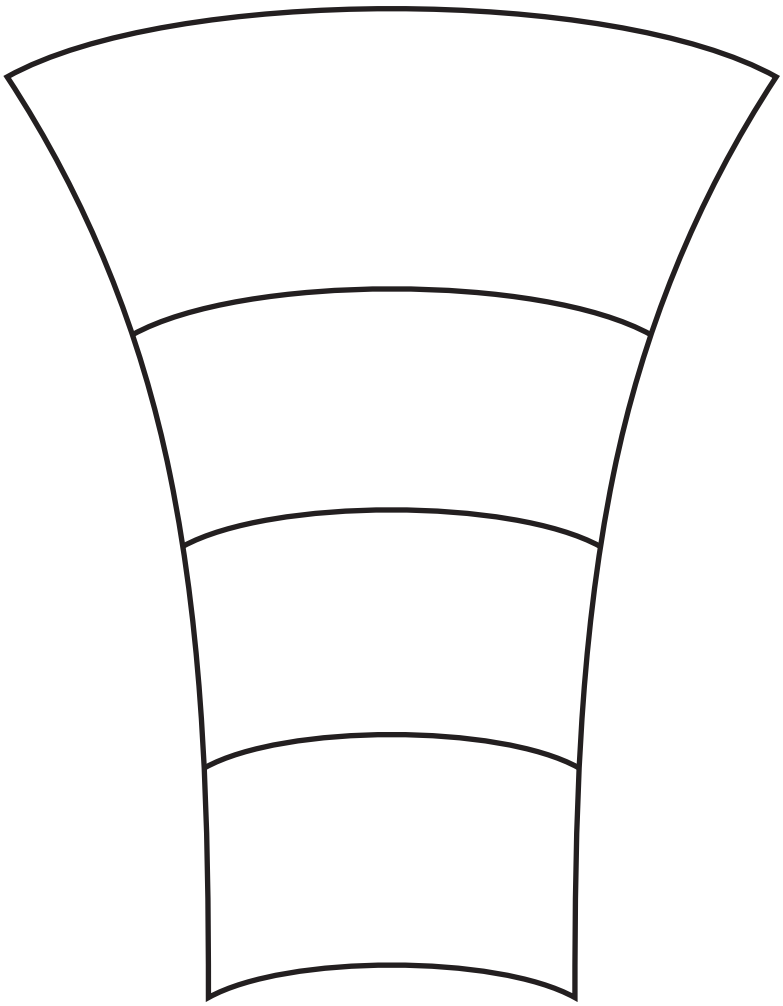

Figure 2. The ladder lattice.

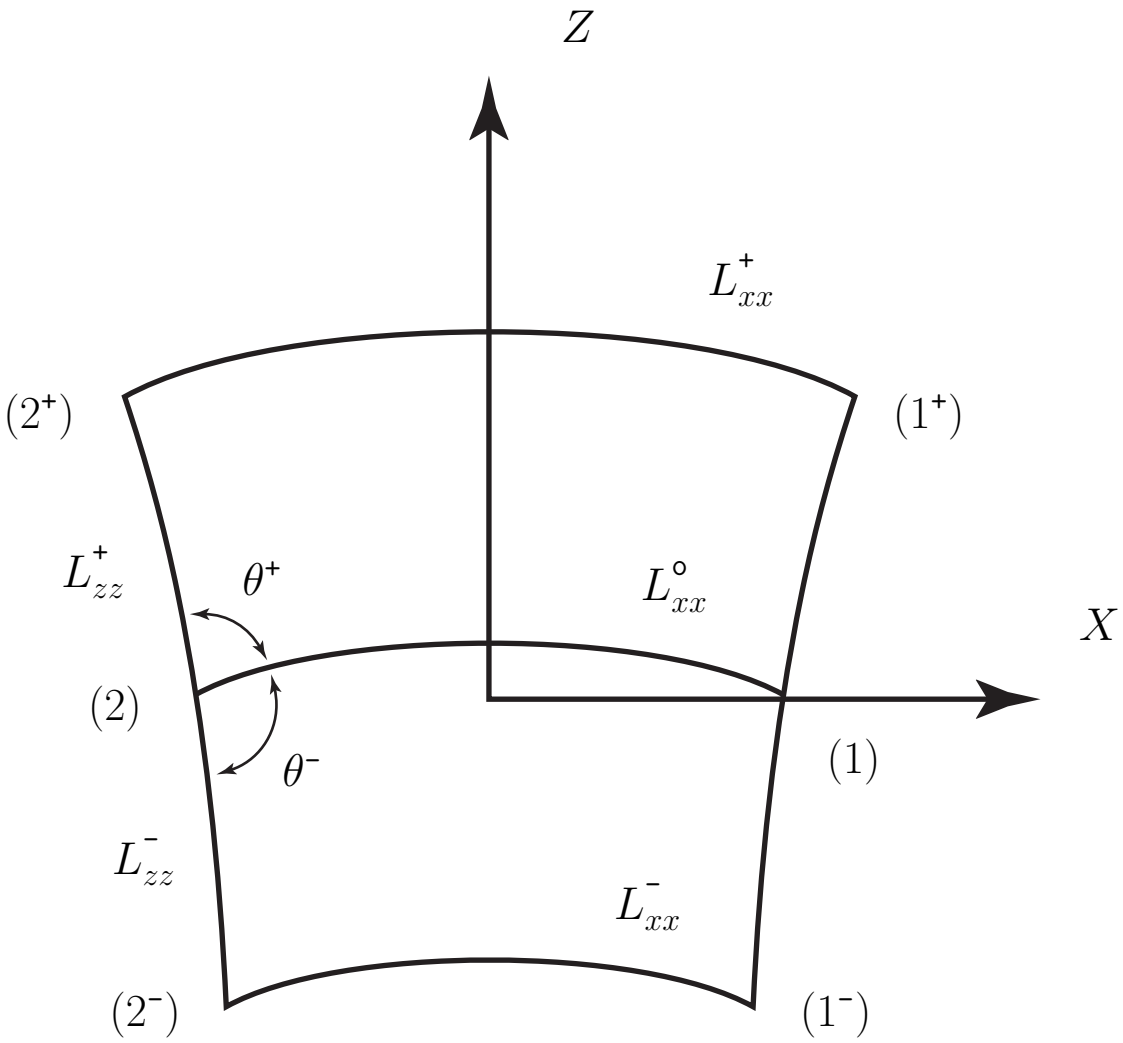

Figure 3. The typical computational cell.

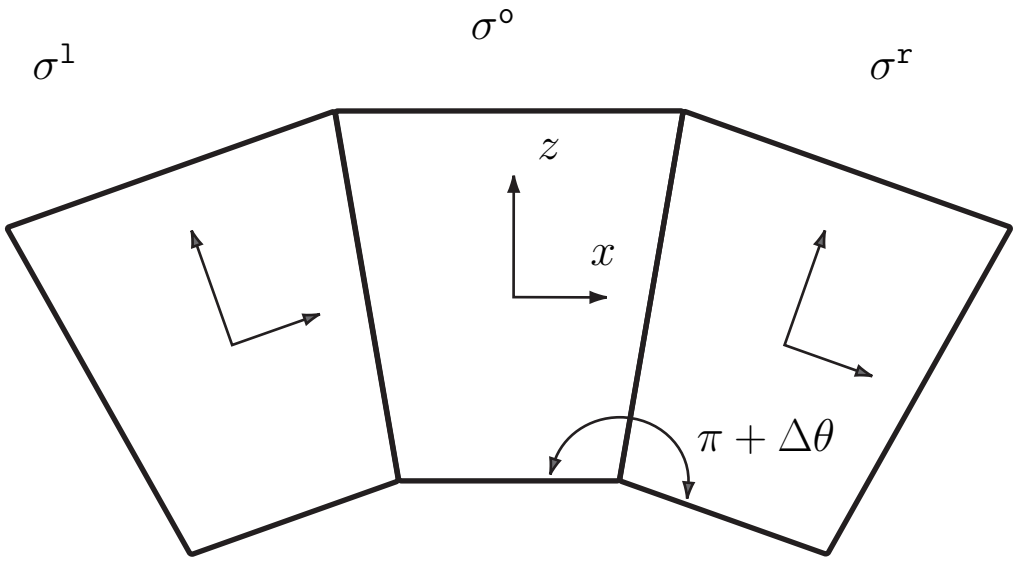

Figure 4. Cells for the Bianchi identities.

Figure 5. Leg lengths

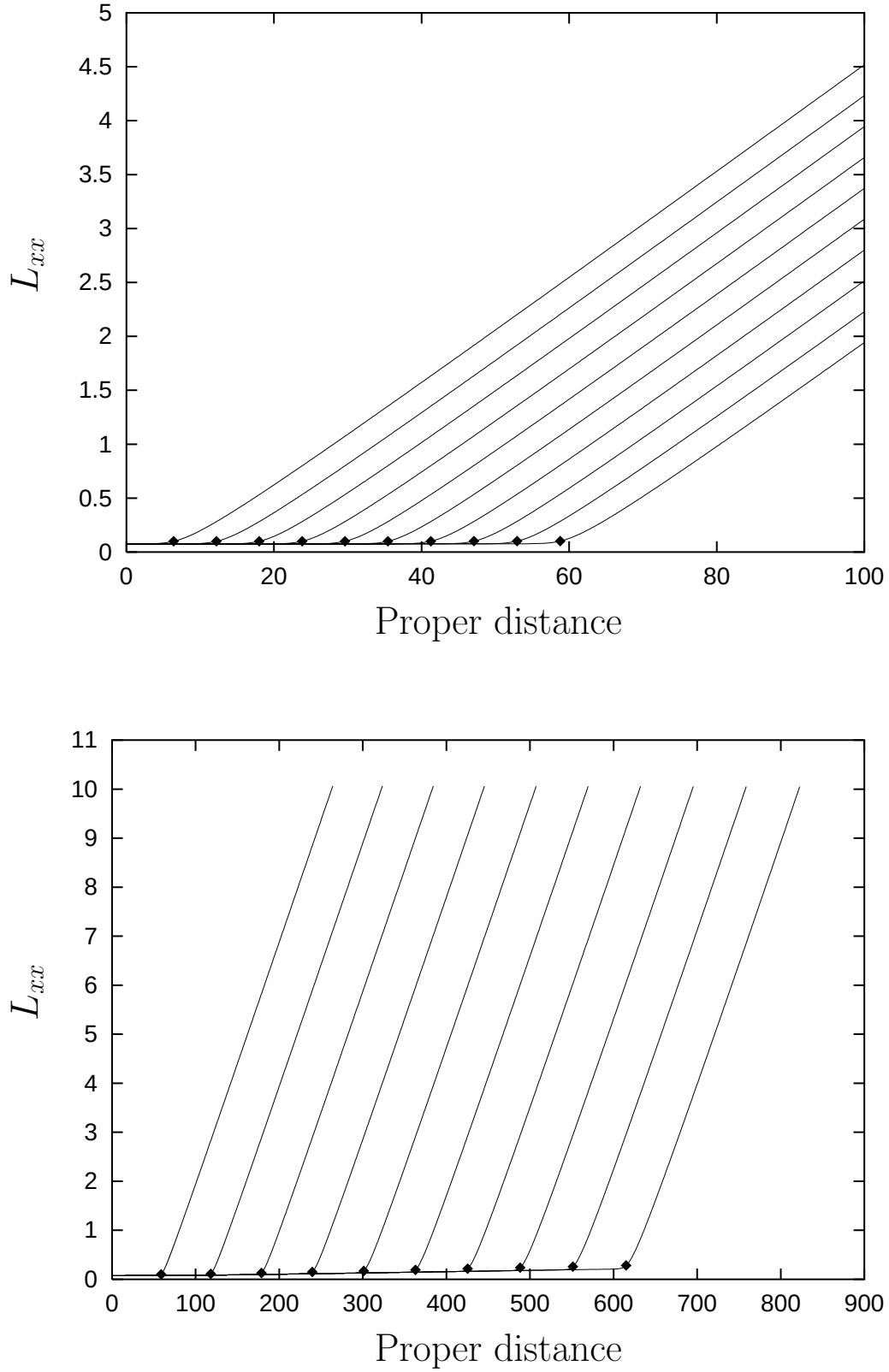

Figure 6. Leg lengths

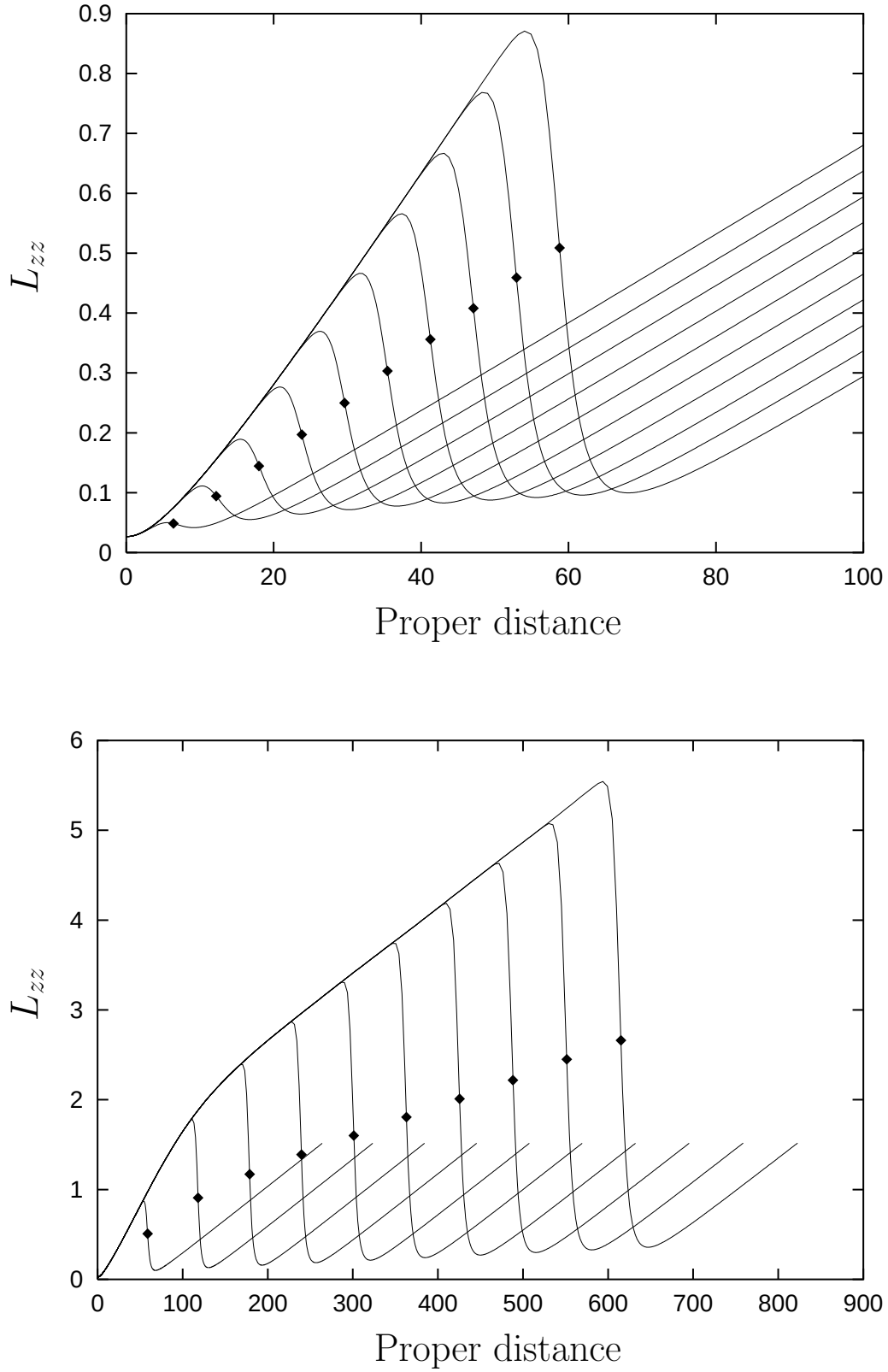

Figure 7. Riemann curvatures

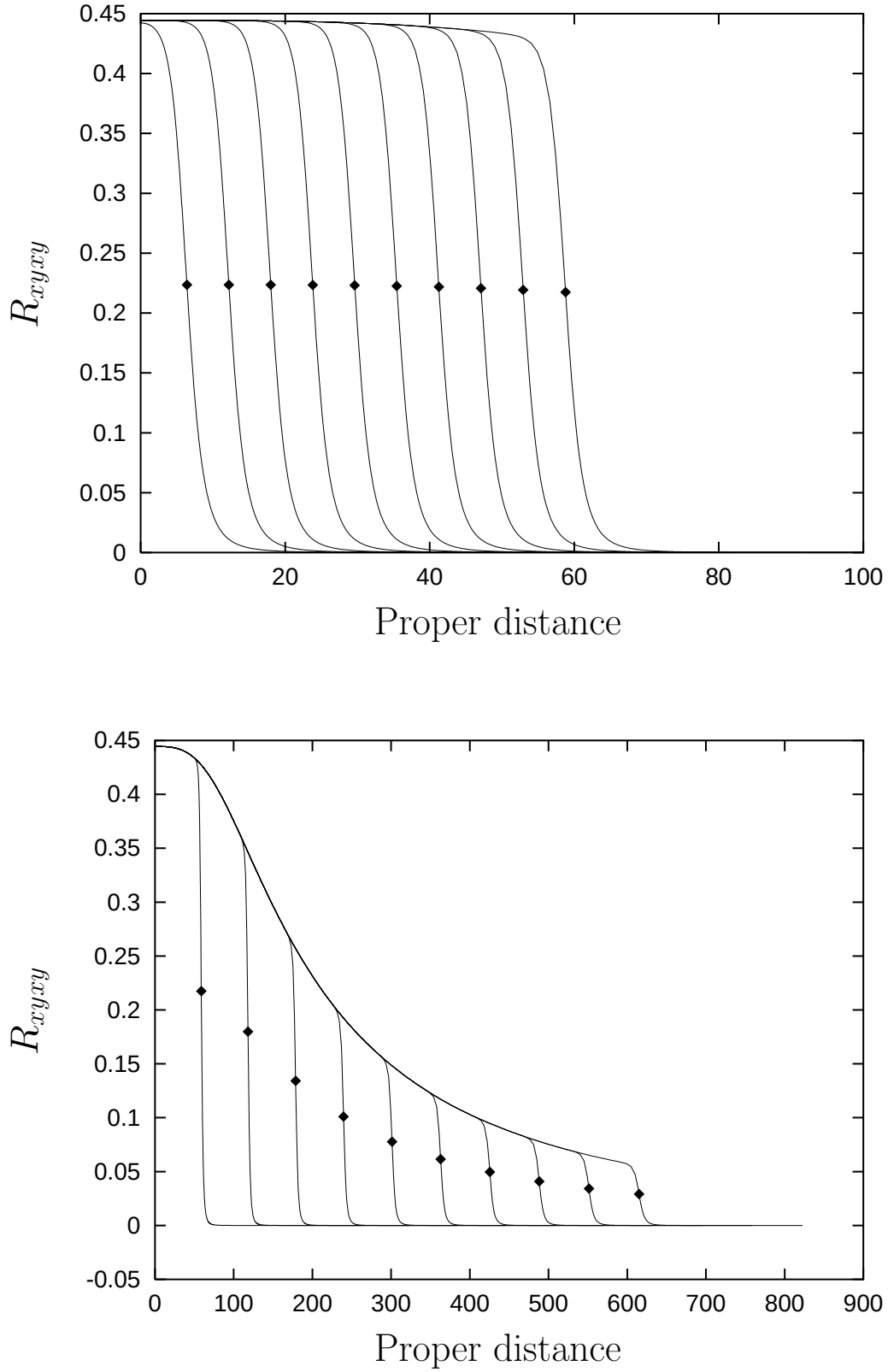

Figure 8. Riemann curvatures

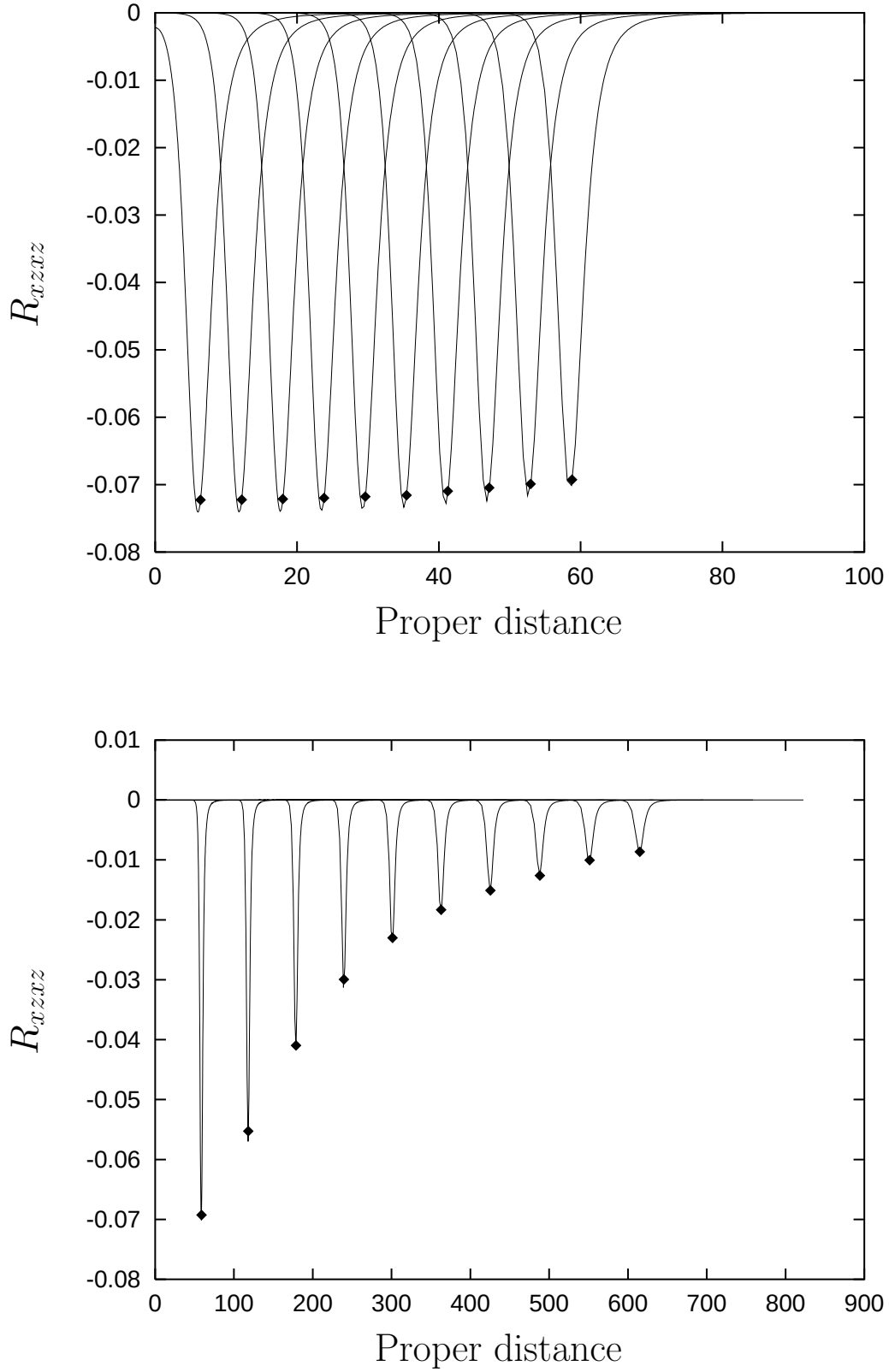

Figure 9. Extrinsic curvatures

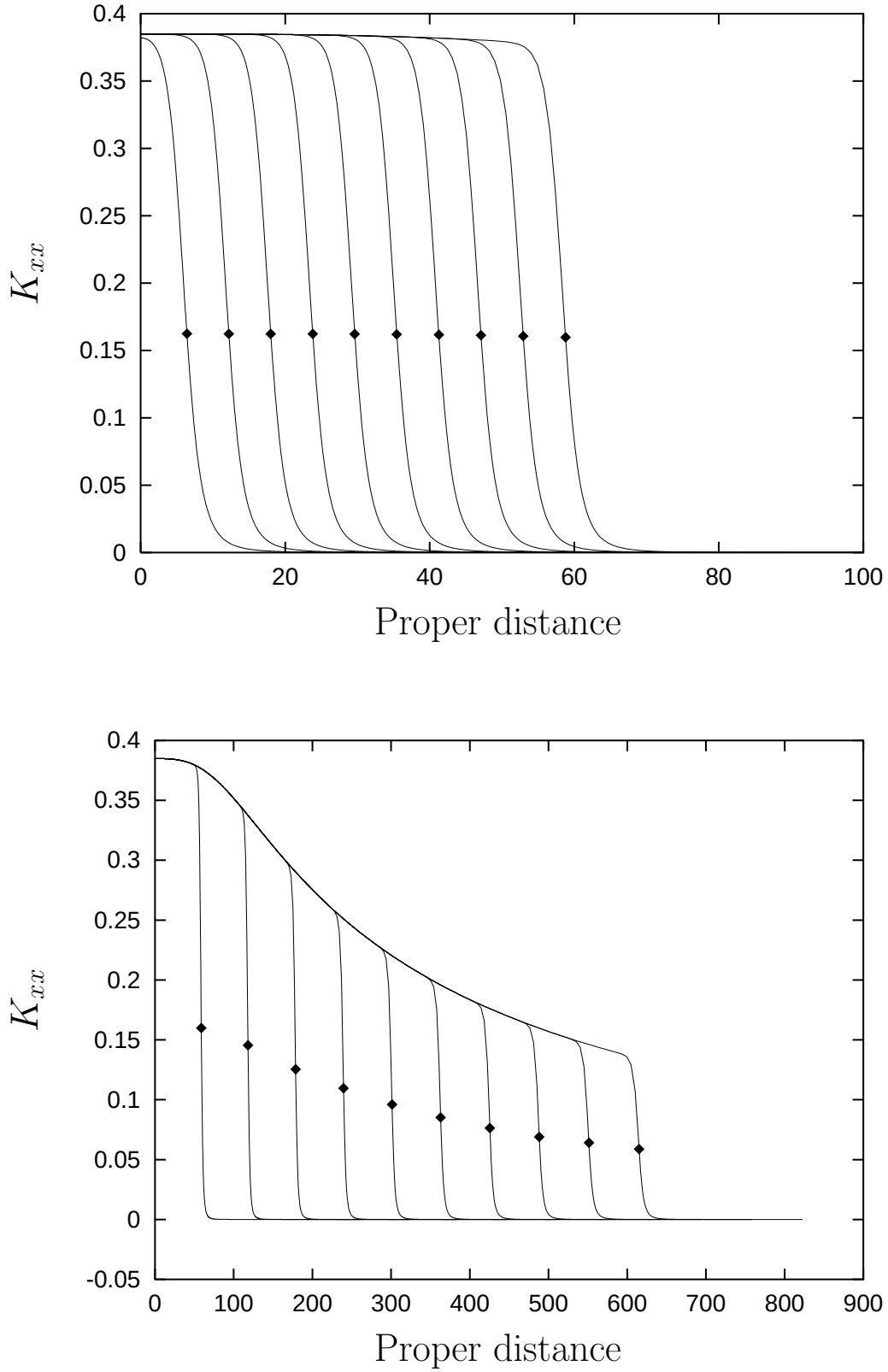

Figure 10. Extrinsic curvatures

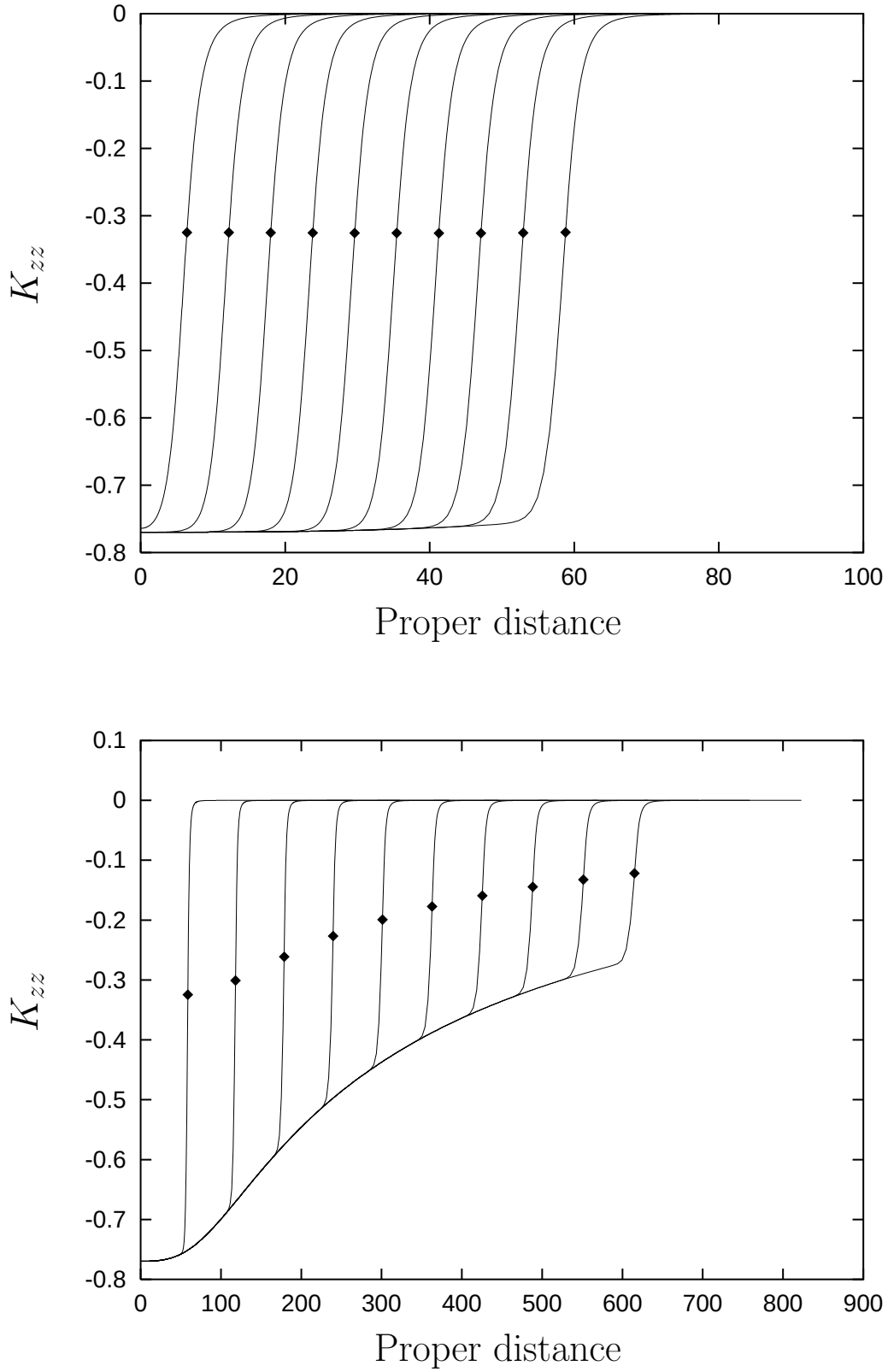

Figure 11. Hamiltonian constraint

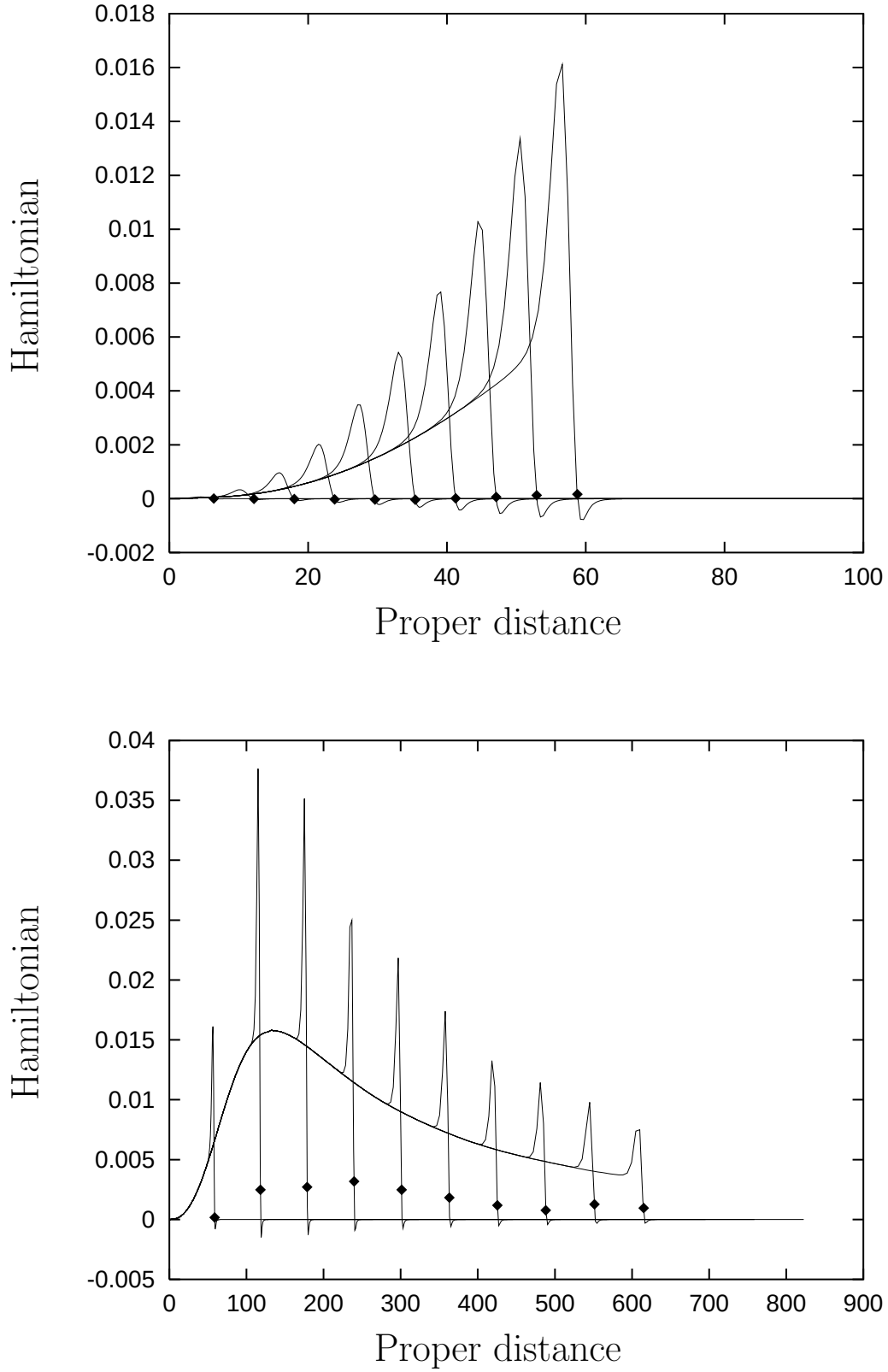

Figure 12. Momentum constraint

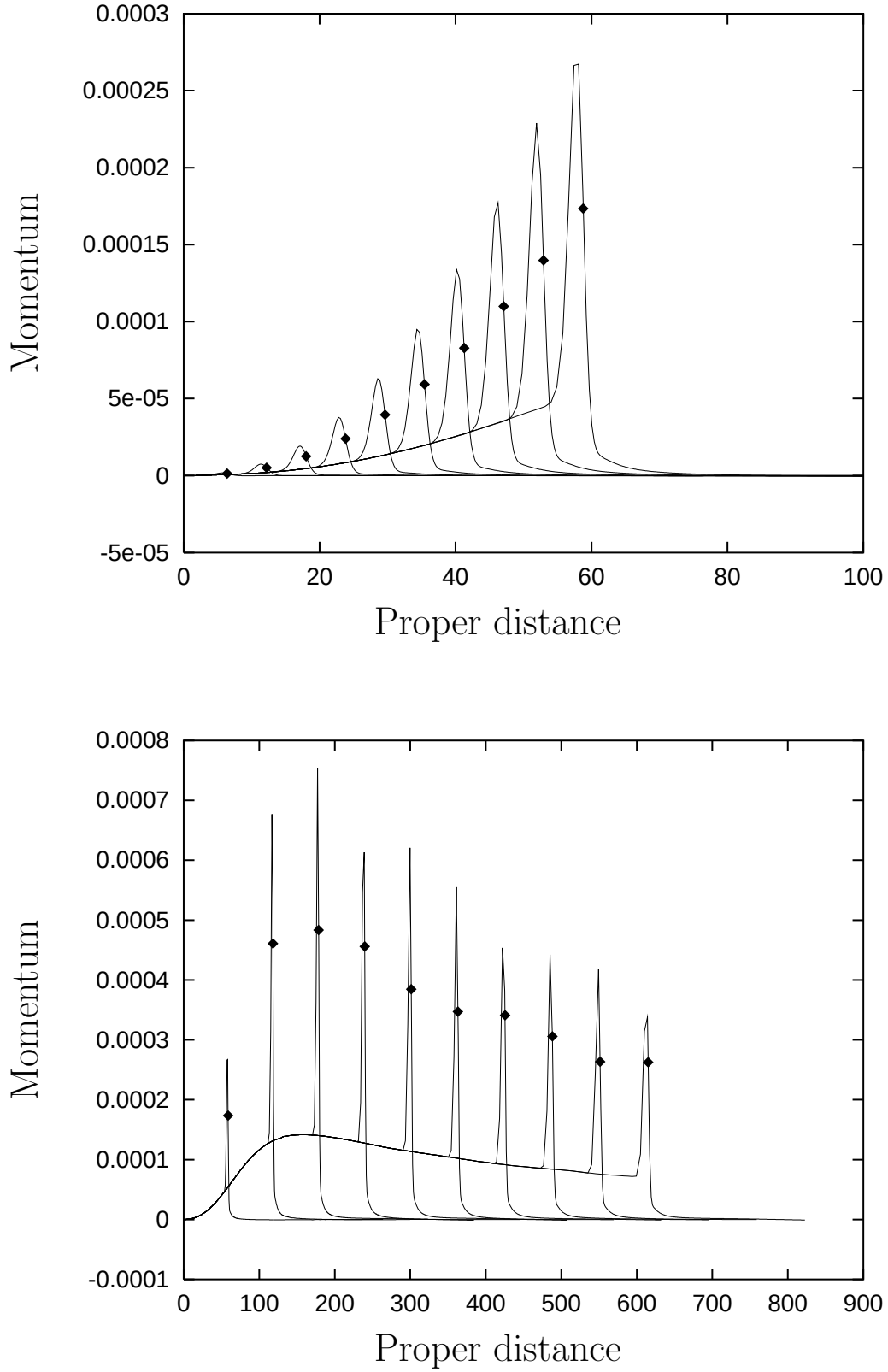

Figure 13. Lapse function

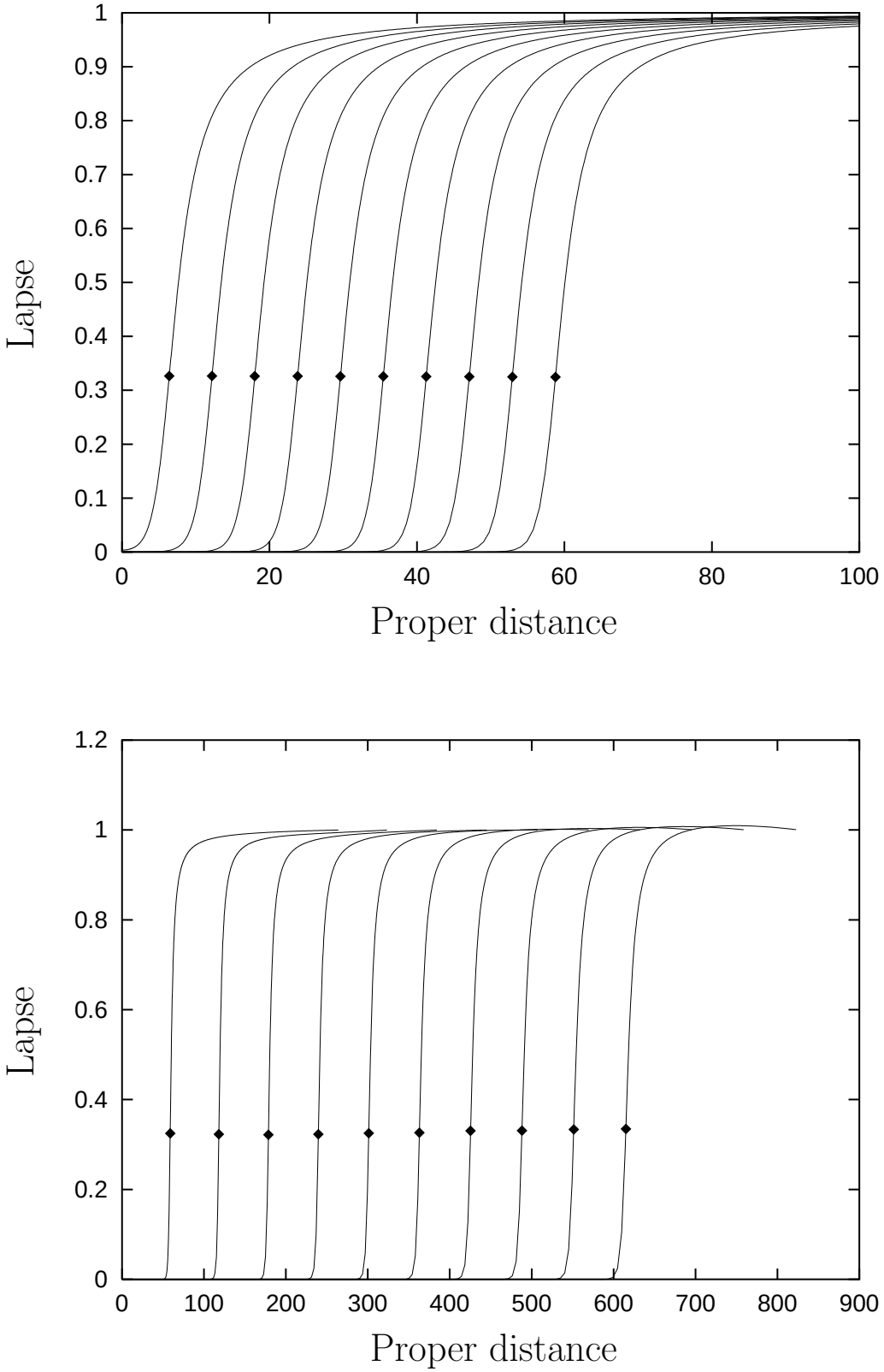

Figure 14. Resolution

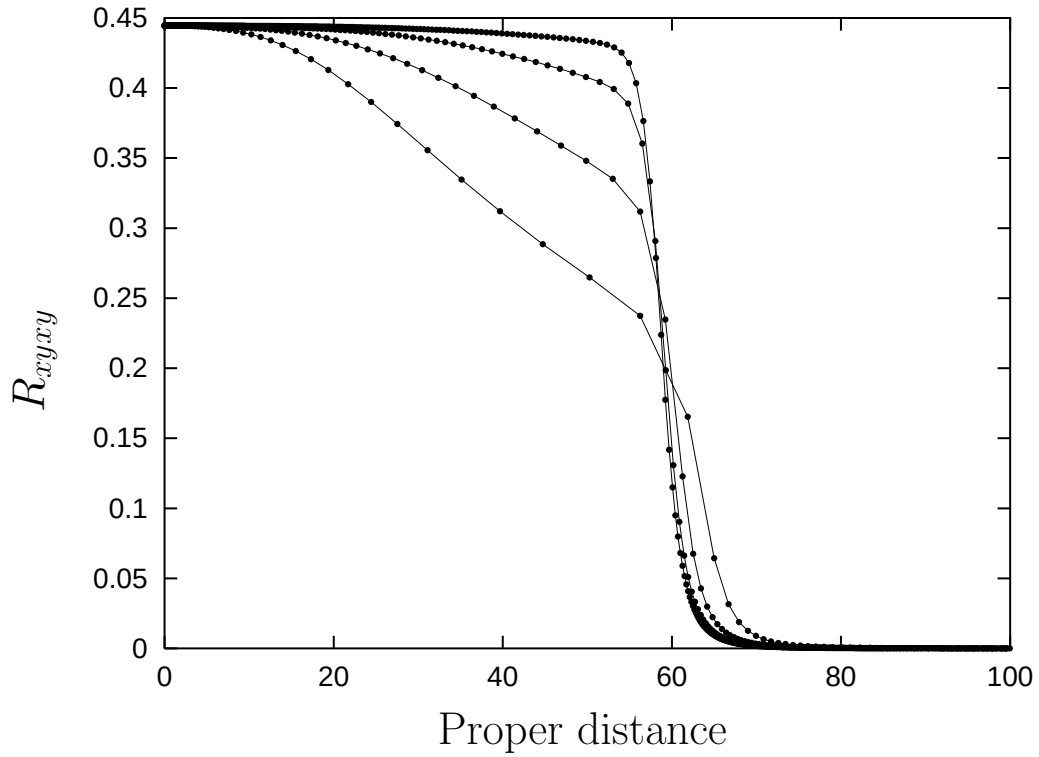

Figure 15. Collapse of the lapse

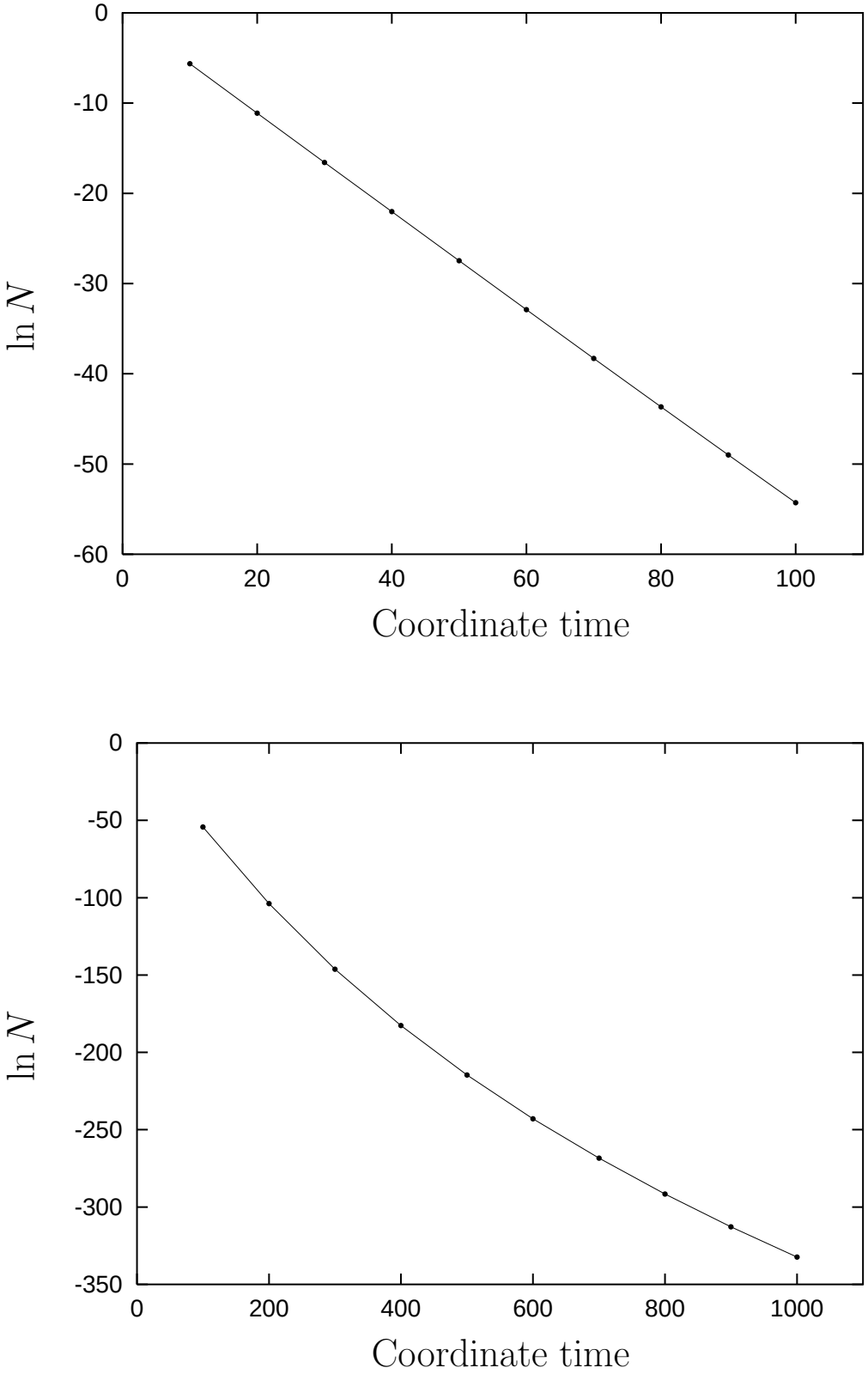

Figure 16. The apparent horizon